DEVELOPING A THREE-DIMENSIONAL (3D) BIOPRINTED TUMOR MODEL

A Thesis

by

BISWADEEP NAYAK

Submitted to the Graduate and Professional School of
Texas A&M University
in partial fulfillment of the requirements for the degree of

MASTER OF SCIENCE

Chair of Committee,	Akhilesh K. Gaharwar
Committee Members,	Isaac M. Adjei
	Kayla J. Bayless
Head of Department,	Michael McShane

December 2021

Major Subject: Biomedical Engineering

ABSTRACT

High phenotypic heterogeneity in tumor cell population, especially with glioblastoma stem cells (GSCs), is one of the major causes of poor prognosis of malignant glioblastoma (GBM). Although *in vivo* drug screening using tumor spheroids and animal models can provide insights about structural heterogeneity, their inability to recapitulate the tumor niche and phenotypic heterogeneity limit their translation to the clinic. Development of an *in vitro* 3D bioengineered model that can recapitulate the native brain niche has the potential to study GBM malignancy. In the present study, we aimed to develop a reproducible bioprinting method to fabricate a physiologically relevant biomimetic GBM tumor model. Towards this aim, we synthesized a brain extracellular matrix (ECM) mimicking gelatin methacrylate (GelMA) bioink with modulated concentration of chondroitin sulfate (CS), a major source of glycosaminoglycans (GAGs) in the brain tissue. Bioprinted constructs of GBM spheroids with integrated brain-specific microenvironmental cues showed intact morphology, high viability and metabolic activity, and enhanced invasion.

DEDICATION

I dedicate this to my mother, Mrs. Basanti Das and my father, Mr. Prasanta Kumar Nayak, for always believing in me and supporting me, no matter the situation. I owe them everything.

ACKNOWLEDGEMENTS

I would like to thank my committee chair, Dr. Akhilesh Gaharwar, and my committee members, Dr. Isaac Adjei, and Dr. Kayla Bayless, for their guidance and support throughout the course of this research. My sincere thanks and gratitude also goes to our collaborator, Dr. Irtisha Singh, for her valuable inputs and counsel in this project, and Dr. Thuy-Uyen Nguyen for her help and guidance with culturing GSCs and verifying their multipotency. I would also like to thank Dr. Kristen Maitland, Director of Graduate Programs and Dr. Michael McShane, Head of Biomedical Engineering Department at Texas A&M University for their help and support.

I would also like to thank my lab mates in the Gaharwar Lab: Shreedevi, Kaivalya, Patrick, Abhay, Aparna, Anna B, Giriraj, and Anna K, for their help and valuable input. A big thanks to all my friends, especially Natalie, Madison, Sarah, Bethany, Siddhant, Agniva, Rahul, and Sridevi, and the department faculty and staff for making my time at Texas A&M University a great experience.

CONTRIBUTORS AND FUNDING SOURCES

Contributors

This work was closely supervised by Dr. Akhilesh Gaharwar, the Department of Biomedical Engineering in collaboration with Dr. Irtisha Singh of Texas A&M Health Science Center at Texas A&M University. Dr. Thuy-Uyen Nguyen, postdoc in Drs. Gaharwar and Singh labs, provided guidance and helped in data collection that is presented in this thesis. The MS thesis committee members Dr. Isaac Adjei, of the Department of Biomedical Engineering, and Dr. Kayla Bayless, of Texas A&M Health Science Center at Texas A&M University provided guidance during this project. All the research work and data contained in the thesis was done by the student under the supervision of Drs. Gaharwar, Singh and Nguyen. I would like to thank all the members of the Gaharwar lab for their help, useful discussions and suggestions.

Funding Sources

Graduate study was financially supported by Dr. Gaharwar (National Institute of Health) and Dr. Singh (Start-up funds).

NOMENCLATURE

GSC	Glioblastoma Stem Cell
GBM	Glioblastoma
ECM	Extracellular Matrix
TME	Tumor Microenvironment
GelMA	Gelatin Methacrylate
CSMA	Chondroitin Sulfate Methacrylate
GAG	Glycosaminoglycan
WHO	World Health Organization
SCID	Severe Combined Immunodeficiency
NSC	Neural Stem Cell
PNN	Perineuronal Nets
CSPG	Chondroitin Sulfate Proteoglycan
CS	Chondroitin Sulfate
CNS	Central Nervous System
3D	Three Dimensional
2D	Two Dimensional
TCPS	Tissue Culture Polystyrene
PVN	Perivascular Niche
CAD	Computer Aided Design
IBB	Inkjet Based Bioprinting
DOD	Droplet on Demand

LAB	Laser Assisted Bioprinting
LIFT	Laser Induced Forward Transfer
MAPLE-DW	Matrix Assisted Pulsed Evaporation Laser Direct Write
DNA	Deoxyribonucleic Acid
MCTS	Multicellular Tumor Spheroids
EBB	Extrusion Based Bioprinting
EMT	Epithelial to Mesenchymal Transition
GAM	Glioblastoma Associated Macrophage
PNIPA	Poly(N-isopropylacrylamide)
PCL	Poly(caprolactone)
PVA	Poly(vinyl alcohol)
HUVEC	Human Umbilical Vein Endothelial Cell
EC	Endothelial Cell
GFP	Green Fluorescent Protein
STL	Standard Tessellation Language
BSA	Bovine Serum Albumin
VEGF	Vascular Endothelial Growth Factor
SDF-1a	Stromal Derived Factor 1a
BK	Bradykinin
PCR	Polymerase Chain Reaction
PBS	Phosphate Buffered Saline
NHS	N-hydroxysuccinimide
EDC	N-(3-dimethylaminopropyl)-N′-ethylcarbodiimide hydrochloride

EGF	Epidermal Growth Factor
FGF	Fibroblast Growth Factor
hr	Hour
min	Minute
sec	Second

TABLE OF CONTENTS

LIST OF FIGURES

LIST OF TABLES

Page

CHAPTER I

INTRODUCTION

Glioblastoma

Glioblastoma is the most aggressive and commonly diagnosed malignant brain tumor worldwide, with an estimated 250,000 new cases and 200,000 deaths in 2020.[1] According to WHO statistics (Globocan 2020), United States reported around 13,000 new cases and 10,000 deaths from glioblastoma in the year 2020 alone.[2] For GBM, the median survival time, which reflects the length of time for which half the diagnosed patients will survive after the start of treatment, is about 14.6 months.[3] Despite being identified in the 1920s, there has been little improvement in the treatment of this disease, as characterized by the relatively unchanged five-year survival times and mortality rates. Moreover, with snowballing population and increasing life spans, the global burden of glioblastoma is also increasing.

Glioblastomas arising from neuroglial progenitor cells are classified into two distinct subgroups, IDH-wild-type and IDH-mutant.[4] IDH-wild-type glioblastoma, diagnosed in 90% of GBM patients, is referred to as primary glioblastoma, and is identified by *de novo* progression with no discernible precursor lesion. IDH-mutant or secondary glioblastoma on the other hand, is characterized by precursor diffusion or anaplastic astrocytoma. Primary GBM, which is commonly diagnosed in older patients with a median age of 62 years, is more aggressive and has poor prognosis, with a median survival time of 4-6 months.

Current state-of-the-art treatment strategies for glioblastoma include a combination of tumor resection or surgery, radiotherapy, and adjuvant chemotherapy. For clinicians, the standard first step for most primary glioblastomas is the maximal surgical removal of the tumor. Depending on the patient's performance, this step is most likely followed by radiotherapy (60 Gray for 6 weeks) with concomitant cycles of adjuvant temozolomide, based on the pioneering phase 3 trial by Stupp et al.[3] Published in 2005, this trial demonstrated that the median survival time increased by a significant 2.5 months when radiotherapy was accompanied with temozolomide uptake. In addition to this, biodegradable carmustine wafers or Gliadel have also been used as a local chemotherapy in the tumor resection sites for improving patient survival. Researchers, in a randomized placebo controlled trial, showed that the median survival of GBM patients increased by 7.5 weeks with implantation of Gliadel wafers post-surgery.[5] While treatment options in primary GBM are well defined, there's no established therapeutic strategy for recurrent GBM. Despite similar options of further resection, reirradiation and symptomatic therapy, there's little evidence of them improving overall survival in patients.

Cancer researchers and pharmaceutical industries have been working together towards developing novel anticancer agents. Despite the intense efforts by researchers in the drug development industry, only a minimal percentage (10%) of drugs tested positive in Phase 1 of clinical trials succeed to gain approval in later stages.[6] Such high drug failure rates could be due to multiple reasons such as erratic clinical trial designs, tumor heterogeneity and use of traditional model systems that are poor representatives of tumors in patients. Since the advent of US National Cancer Institute anticancer drug screen, most of the pre-clinical strategies of drug screening have been based on 2D cultures and animal models. Although both these model

systems have been immensely helpful in understanding cancer biology, their inability to represent patient tumors has been perceived to be responsible for the high failure rates of anti-cancer drugs as they move from pre-clinical to human trials.[7] Since the time and resources consumed in this entire process are enormous, it becomes pivotal to gain accurate insights into various molecular mechanisms involved in tumor progression, maintenance, invasion, and therapeutic resistance prior to the drug development process. Over the past few decades, researchers have adopted numerous novel strategies to create reliable, robust and predictable *in vitro* culture platforms that can recapitulate the original properties of the *in vivo* tumor.

Glioblastoma stem-like cells

According to the cancer stem-cell hypothesis, there exists a small subpopulation of self-renewing cancer cells that are responsible for initiation, maintenance and progression of cancer.[8] Cancer stem cells were first identified based on their ability to initiate acute myeloid leukemia in SCID mice.[9] Since then, they have been identified from various solid tumors by the prevalence of different cluster of differentiation markers, e.g. $CD133^+$ in glioblastoma.[10] In fact, GSCs were first identified from brain tumors by their expression of $CD133^+$ and were shown to possess the properties of self-renewal and multipotency. The ontogeny of GBM has been a hot topic of discussion in the scientific community with no concrete conclusions thus far. Multiple studies have highlighted an overlay between gene expression profiles of neural progenitor cells and glioblastomas, that suggests the presence of conserved cell signalling pathways in normal and malignant neural stem cells.[11, 12] However, whether GSCs arise from neural stem cells after certain mutations or from a mature and differentiated cell type that acquires self-renewal

properties is yet to be determined. Regardless of GSC ontogeny, they are known to be deceptive and promote survival of malignant tissue, as opposed to repairing damaged tissue, like “normal” neural stem cells, and the knowledge of this GSC characteristic holds great value as it can be exploited to develop new therapies against glioblastoma.

In the recent years, targeting glioblastoma stem-like cells has been proposed as a promising strategy to treat malignant glioblastoma. Multiple studies have held GSCs accountable for the aggressiveness and evasiveness of this disease in various *in vitro* models.[13-15] GSCs are known to promote therapy resistance and intratumoral heterogeneity in glioblastomas.[16] Distinct signaling pathways that play a key role in enhancing the aggressiveness and resilience of GSCs have been identified. GSCs drive their characteristic features by enhancing the genetic instability of the tumor, leading to various mutations in pivotal replicative checkpoints such as p53, NF1, ATRX, and TERT.[16, 17] These mutations, quite paradoxically, enhance GSCs ability to repair damaged DNA by upregulating various checkpoint kinases such as Chk1, Chk2, and repair enzymes such as PARP1 and TIE2.[18, 19] Pathways which are generally associated with maintaining cancer stemness, such as the NOTCH signaling pathway, have also been reported to mediate GSC survival and therapy resistance by upregulating PI3K/AKT and Bcl-2 pathways.[20] Finally, the inherent heterogeneity in the genetic and epigenetic landscape of GSCs, creates a highly versatile system that can still thrive and function at the cost of failure of a few components due to specific therapeutic targeting.

Evidently, GSCs are crucial for the survival and maintenance of GBM. Thus, therapies that can target these cells and inhibit their pro-tumorigenic functions could prove highly

effective. However, in order to develop such therapies that are effective and efficient, we need a deeper understanding of GSCs' functions, their interactions with the tumor microenvironment and its consequences towards promoting tumor survival in a physiologically accurate setting.

Tumor microenvironment

Previous studies have shown that normal stem cells are highly regulated by the stem cell niche.[21] Similar to neural stem cells, GSCs also depend on microenvironmental cues for their survival and function. For instance, McCord et al. have highlighted the prevalence of GSCs in a hypoxic microenvironment and its role in regulating their self-renewal.[22] Similarly, acidosis, which is often a consequence of hypoxia, is also known to upregulate the expression of stem cell markers like Oct4, Olig2, and Nanog and promotes GSC phenotype.[23] High-grade gliomas grow in a dynamic microenvironment with extensive extracellular matrix proteins and various stromal cells, including endothelial cells, pericytes, microglia, astrocytes, neural stem cells and peripheral immune cells.[24] Microvascular hyperplasia, which is characterized by highly proliferating brain endothelial cells that form aggregates in a vascularized GBM tumor, is the first step in creating a perivascular niche (PVN), that supports GSC survival in multiple ways. As discussed in a detailed review by Schiffer et al., this perivascular niche plays multiple crucial roles in facilitating tumor growth, progression, invasion and recurrence.[25] Here, in the context of this study, the importance of tumor ECM, specifically proteoglycans, and the perivascular niche, towards tumor growth and prevalence will be discussed.

Proteoglycans: A key component in the brain ECM

The ECM components of the central nervous system are localized in three compartments: the basement membrane, the perineuronal nets (PNNs) and the interstitial matrix. The basement membrane, which serves as a boundary between vasculature and interstitium, is primarily made of collagen, entactin, fibronectin, and perlecan. The perineuronal mesh-like nets, which preserve neuronal health and synaptic plasticity, are typically composed of proteoglycans, and tenascin R. The neural interstitial matrix, which sequesters signalling molecules like growth factors and morphogens, is comprised of hyaluronan, tenascins, proteoglycans, and relatively lower amounts of fibrous proteins like collagen, laminin and fibronectin.

Proteoglycans, which are made up of proteins (from *'proteo'*) with attached unbranched glycosaminoglycan (from *'glycan'*) side chains, are an essential component of the tumor ECM. Different proteoglycans vary in the constitution of their base protein and/or the type of GAG side chains. GAGs are long negatively charged polysaccharide chains of repeating disaccharide units. Based on the molecular composition of the disaccharide, they are classified into heparin sulfate (HSGAGs), chondroitin sulfate (CSGAGs), keratan sulfate and hyaluronic acid glycosaminoglycans. Among these, CSGAGs represent a major class of GAGs, which play a pivotal role during neuronal development, nerve plasticity, formation of PNNs and tissue damage repair.[26] However, abnormal expression of proteoglycans has been characterized as a hallmark of multiple malignant tumors.[27] Moreover, as claimed by The Cancer Genome Atlas (http://cancergenome.nih.gov/), the upregulation of many chondroitin sulfate synthases is a characteristic feature of GBM.[28] CS proteoglycan (CSPG), which is a crucial prognostic marker

for this disease, has been reported by multiple researchers to enhance the development, progression and therapy resistance in gliomas.[29-31] So, that being the case, we hypothesized that the incorporation of chondroitin sulfate in the bioink to mimic the pro-tumorigenic niche will recapitulate the invasion pattern like native GBM. As per our knowledge, chondroitin sulfate is the most inexpensive source of GAGs that is commercially available, and can be easily functionalized with methacrylate groups that make it photo-polymerizable. Methacrylate chondroitin sulfate or CSMA has also been shown to possess good 3D print fidelity by multiple groups for various applications such as cancer modelling, and cartilage tissue engineering.[32, 33] Together, these were the driving factors for us to choose chondroitin sulfate for our application over other GAGs.

The perivascular niche in GBM

Glioblastomas are highly vascular tumors and this vasculature complements their malignancy well. Evidently, glioblastomas are known to create and exist in a perivascular niche which is composed mainly of endothelial cells, pericytes, and astrocytes, to support their survival and proliferation.[24] This niche has gained increasing attention over the years, both in normal and malignant brain tissue, due to its physiological and pathological functional implications as mentioned below.

High-grade glioma vasculature is characterized by two crucial histological markers, microvascular proliferation and endothelial hyperplasia. High microvascular proliferation is showcased by the increase in proliferative activity of pericytic, endothelial, and vascular smooth

muscle cells. Tumor neovascularization is often correlated with the higher prevalence of these microvascular structures, which play a crucial role in enhancing GBM malignancy. The high angiogenic niche regions thus formed, are at the centre of function for ensuring the localization and survival of GSCs and maintenance of their stemness.[34] On top of that, multiple molecular signalling pathways are upregulated in the perivascular niche, indicative of the cellular crosstalk between endothelial and stromal cells to support GSCs growth and function.[35] Multiple groups have revealed that GSCs contribute to neovascularization in GBM by differentiating into pericytes and endothelial cells, in a phenomenon well known as vascular mimicry.[36-38] Pietras et al. have also reported the close association of GSCs and vasculature and the role of endothelial derived factors to preserve GSC stemness.[39] Together, this evidence suggests the key role of the perivascular niche in facilitating tumor progression by regulating crucial cell to cell signalling. Understanding the underlying mechanisms that control GSC activity in the brain PVN could prove fruitful towards designing new therapies.

Current methods to study GBM

Two-dimensional (2D) monolayer cultures have been popular *in vitro* models to understand GBM biology due to their inexpensiveness and ease of availability and experimentation. U87, U251, and T98G are some of the GBM cell lines that have been cultured in monolayers in 2D TCPS plates to understand molecular pathways involved in the progression of this disease.[40] For example, past studies by Lakka et al. used 2D monolayer GBM cultures to elucidate the role of cathepsins and MMPs in tumor growth, invasion and angiogenesis.[41] In another pivotal study, Kenig et al. used U87 cell line to demonstrate the role SDF-1 mediated

crosstalk between gliomas and endothelial cells in enhancing tumor proliferation and invasion.[42] However, when cells are cultured on 2D tissue culture polystyrene (TCPS), they attain a flat morphology and lose a majority of cell-cell and cell-extracellular matrix (ECM) interactions. As a result, most of the ECM-mediated signaling is abrogated and the cellular response to various stimuli is different to their responses *in vivo*. Reports suggest that the tumors formed by implanting these cells cultured in monolayers fail to recapitulate the characteristics of the native GBM tumor.[43]

To overcome these limitations, xenografts of patient-derived GBM cells have been routinely used to recapitulate the biological and genetic features of original tumors and understand cancer biology. However, animal models have low engraftment rates and require a long time (2-12 months) to be established. In addition, the stromal biology varies i.e. the human stroma in the tumor is replaced with murine stroma after engraftment, thus changing the original characteristics of the tumor, resulting in an altered physiological response in the host animal.[44] Also, since this approach involves the production and maintenance of genetically engineered mice, it makes this approach significantly expensive, time consuming and laborious. Due to these reasons, three-dimensional (3D) engineered cultures have evolved to be a more promising tool to fabricate GBM models. The key advantage of such models over 2D monolayer cultures, and xenograft models, is that they can be tailored to provide the appropriate tumor microenvironment, thereby creating an organotypic platform for studying cancer biology.[45]

Even with 3D models, there are multiple ways to fabricate them which come with their own set of advantages and limitations. 3D matrix models are the most commonly used 3D models that have been used to incorporate gradients of soluble cues, and test variations in topography, stiffness, ECM composition, etc. Matrices made of collagen[46], chondroitin sulfate[47], hyaluronic acid[48], and Matrigel[49] are routinely used for modeling glioblastoma due to their compositional complexity and excellent bioadhesive and biocompatible properties. Synthetic scaffolds that are fabricated using electrospinning and salt leaching techniques from polymers like polystyrene (PS)[50], polycaprolactone (PCL)[51], poly(N-isopropylacrylamide-co-Jeffamine M-1000 acrylamide) (PNJ)[52], have been used to demonstrate the role of matrix cues, stiffness and dimensionality towards GSC survival and maintaining stemness. However, in order to mimic the tumor niche more accurately and improve physiological relevance, additional layers of complexity need to be incorporated. Microfluidic models have been exploited towards this purpose by incorporating crucial parameters like fluid flow, hypoxia gradients, chemical cues, co-culture with stromal cells, and spatial organization. In addition, they have been proven to be low-cost, better for imaging, and capable for high throughput screening than standard *in vitro* 2D and 3D models for clinical applications.[53] For example, Jingyun et al. used a 3D GBM microfluidic model to recapitulate tissue organization, ECM composition, and flow conditions to investigate the proliferation and invasiveness of GBM cells under dynamic therapeutic stress, which would be difficult to achieve via other fabrication tools.[54]

Additive manufacturing for cancer models

3D cancer models are typically fabricated from natural or synthetic polymers, by using numerous methodologies, depending on the requirements of the study.[55] A particularly exciting approach is: 3D printing or additive manufacturing, which refers to the layer by layer deposition of precursor materials to fabricate complex 3D geometries from computer-aided designs (CAD). It has emerged as a promising fabrication tool in the past decade. Over other popular fabrication methods like soft lithography or polymer scaffolds, 3D printing has certain advantages such as increased efficiency, reproducibility, and customizability, achieved either on a small or industrial scale. More recently, it has evolved significantly towards "printing" soft biomaterials, which has furthered the field of tissue engineering, and regenerative medicine, while prospectively allowing researchers to develop exemplary patient-specific cancer models to advance drug screening, and cancer biology. The ability to "print" and mimic physiologically relevant complex 3D architectures of tissues and organs while maintaining or recapitulating cell-cell and cell-ECM interactions at a relatively low cost and higher efficiency is what has rendered this ingenious technology so popular in the scientific community. Hereby termed "bioprinting", this process is readily compatible with fabrication of tissue constructs via conventional sacrificial, and deposition-based workflows. The fabricated tissue structures are composed of cells, ECM and biomaterials deposited with micro-scale precision and have been extended towards building models of breast, brain and pancreatic cancer.[56] However, some limitations still exist which prevent its large scale deployment - these include integration of printed constructs into traditional screening or testing workflow, speed of fabrication, *in vitro* maintenance, and deployment in resource limited settings. Functional understanding of material parameters such as viscosity,

shear thinning, and crosslinking mechanisms is empirically determined. Following this, these intricately linked properties are used to determine process parameters like nozzle gauge, and extrusion speed to develop functional 3D structures. Shear and thermal exposure have been known to compromise fidelity of final structures while affecting cell viability, cell motility, differentiation, and drug resistance. It is, hence, paramount to develop a first principles understanding of the printing process and the effects that living materials imbibed within the ink are subject to.

Bioprinting techniques

Multiple strategies of bioprinting have been utilized for recapitulating the 3D architecture and complexity of biological tissues and organs: inkjet-based, extrusion-based, and laser-assisted bioprinting. Inkjet-based bioprinting (IBB) uses heat or piezoelectric actuation to deposit droplets of bioink at the print bed. On the other hand, extrusion-based bioprinting (EBB) uses either pneumatic or mechanical forces to extrude a stream of bioink from the nozzle. In laser-assisted bioprinting (LAB), cell-laden hydrogels are transferred from a donor film to the print bed via laser-assisted heat transfer. In the following section, fundamental mechanisms of action of the various print methodologies in addition to the big picture goals associated with bioprinting which include; stable biomolecular gradient patterns, scaling from 2D to 3D, pattern integrity and robustness, co-printing of multiple biomaterials and preservation of biological activity along with printing of complex ECM architectures will be covered. The cellular and other materials that are printed, termed as “bioinks”, and the various parameters that affect their printability and functionality will also be discussed.

Inkjet based bioprinting uses pico-liter sized droplets and is generally considered suitable for incorporation of biological elements and their controlled deposition over a defined surface area. The droplet on demand (DOD) technology has garnered attention from the bioprinting community due to its simplicity. The nozzle diameter which can be as small as 20 μm, simply displaces the ink on to the print bed under the application of a controlled pressure pulse. Leaks are prevented by tuning the surface tension of the ink. Heat based actuation or thermal inkjet printing typically increases liquid temperature by about 4-10 °C to produce expanding heat bubbles which are directed towards the nozzle outlet. Thermal inkjet printing is fast and low cost but ultimately print quality is hard to control due to instability of the ejected heated bubbles. Additionally, optimal control over ink viscosity and maintenance within optimal ranges is required to limit decreases in cell viability. Piezo-electric actuation consists of deformation of the ceramic chamber wall by a voltage pulse that results in a rapid volume change and droplet ejection. Droplet printing efficacy is evaluated by observing parameters such as: droplet velocity, consistency and shape. As no heat is involved, Piezo-electric actuation does not produce heat related damage of cells and biological materials. However, the major modes of cell damage that need to be considered are sonication and shear related damage of cells when ejected.

A significant downside of the inkjet printing process is the low viscosity and mechanical strength of printed constructs. Hence, they need to be combined with traditional methods such as electrospinning, extrusion-based approaches with addition of peptides and copolymer blends for mechanical reinforcement. As such, future work is being directed towards broadening the range of printable bioinks by overcoming the current bottlenecks associated with failed geometry

retention and better functional support for robust 3D structures. Finally, the applicability of inkjet bioprinting is remarkably limited due to the lack of a specialized inkjet bioprinter, which is undersupplied due to the configuration complexity of its flow channel, high precision need for micro-machining, and low longevity of the inkjet head.

Among available bioprinting techniques, laser-assisted bioprinting (LAB) is an up-and-coming technique due to its high resolution, improved cell viability, and the ability to print high-viscosity bioinks. Matrix assisted pulsed evaporation laser direct write (MAPLE-DW) and laser induced forward transfer (LIFT) are the two most common modes of LAB. The two modes have shown promise in printing biomaterials such as protein and DNA.[57, 58] MAPLE-DW involves bioink processing in ambient air, where the laser beam transfers a micrometer-dimension amount of bioink to the substrate. On the other hand, a typical LIFT bioprinting system comprises of a laser source, donor ribbon, and a collector substrate. The process of laser printing can be broken down into three parts: (1) utilization of a high energy laser pulse to a thin biomaterial layer, (2) high-pressure bubble production, and (3) discharge of a bioink droplet. The excitation of the bioink results in a large increase in temperature within a little volume of the bioink which is followed by high pressure bubble generation at the bioink layer. The bubble expands vertically, and a pressure gradient is developed across the stream. Upon reaching critical pressure, the bubble collapses resulting in deposition of the ink on the base substrate.[59] Near-Infrared lasers are preferred due to their non-interference with the physico-chemical properties of the bioinks, in addition to light UV~93 nm with pulse frequencies in the femto and nano second range.[60] Rheological properties of the bioink affect size of the bubbles which in turn affect the printed dimensions.

LAB has been used to develop *in vitro* cancer models with features like the tumor microenvironment being used to faithfully replicate its biological function. In one report, MAPLE-DW LAB was used to print hydrogels microbeads with breast cancer cells into spatially defined patterns in hydrogel matrices containing differentiated adipocytes.[61] In a follow up, multi cellular tumor spheroids (MCTS) composed of cancer and embryonic stems cells of varying densities were seeded by controlling the laser pulse and cell seeding density on the printed ribbon. However, even furnishes with a high-frequency laser, the productiveness of LAB cannot compete with other bioprinting methods, such as the inkjet and extrusion-based bioprinting.

Extrusion bioprinting is the most common mode for tissue fabrication, in which living constructs are manufactured additively via layer-by-layer deposition of cell-incorporated bioinks. The mechanisms of actuation can be roughly characterized into screw, piston and pneumatic modes. Pneumatic systems extrude the bioink by using compressed air as the driving force, and they perform better with high viscosity bioink. However, there can be a slight delay in extrusion due to the need for prior gas compression. On the other hand, piston-driven systems provide better command over the fluid flow from the nozzle, and screw-based systems impart finer spatial control. However, one issue with made-to-order screw-driven systems is the substantial drop in pressure at the nozzle, which hampers cell viability. To sort out this issue, often, the extruder is and needs to be customized for bioprinting.

Hydrogel inspired bioinks are the central component of the printing process and must meet certain physicochemical characteristics to ensure maintenance of a hospitable environment

for all living materials during printing as well as culturing process. Extruder bioprinters are capable of printing bioink with a wide range of viscosities from 6 to 30 million mPa·s, with various cell densities and even cell aggregates and organoids. However, a decrease in cell viability by 10-20% might be observed due to the high cell stress during printing.[62] Printing resolutions that can be achieved comfortably have been reported to be in the range of 100-200 μm.

As cell-cell interactions, cell-biomolecule interactions are the prime focus of most mechanistic cancer studies, extrusion based bioprinting's primacy in the bioprinting of cancer model hierarchies remains unchallenged. Complex geometrical architectures with relatively facile tuning of process parameters have been studied.[63] One of the earlier reports utilizing EBB for cancer bioprinting by Xu et. al consisted of extruding ovarian cancer cells and human fibroblasts on Matrigel in different patterns.[64] Extrusion afforded high degrees of spatial control over deposition of cancer cells allowing for increased repeatability over traditional pipetting methods. High cell viabilities of over 90% were obtained with this trend being maintained as cells continued to proliferate post-patterning. Van Pel used 3D bioprinting, and combined scaffold-free, self-assembled human glioma cell spheroids and mouse neural progenitor cell-derived spheroids to follow glioma cells invasion into neural like tissue in fixed samples and in real time.[65] Wang et al. enriched glioma stem cells in 3D EBB scaffold free tumor model and investigated epithelial mesenchymal transition (EMT) with the cultured stem cells showing increased stemness in vitro an increased tumorigenicity in-vivo.[66] Heinrich et al. studied the various interactions between glioblastoma cells and macrophages and the effects of putative therapeutics on these interactions in bioprinted mini-brain tissues.[67] They concluded that

glioblastoma-associated macrophages (GAMs) were being recruited by GBM cells and which polarized them into a GAM-specific phenotype. They were able to demonstrate that extrusion bioprinting can be used to create a controlled microenvironment, in a complex 3D geometry which would be difficult to achieve with the traditional 2D *in vitro* cancer models. The aforementioned platforms used extrusion to develop pseudo-realistic expression of the tumor microenvironment (TME), which might help generate clinically useful insights into disease progression and elucidate new target mechanisms for cancer drugs.

Bioink formulations

Designing bioinks is an important part of the bioprinting process as most native formulations rarely have both, the physico-mechanical properties required for printing and the biochemical signals to cater the biologic necessities of the incorporated cells. Moreover, these properties do not go hand-in-hand very often. For instance, a high-viscosity bioink will have smooth extrusion of filament while supporting the subsequently deposited layers showing structural solidity. But, this high-density bioink may lead to stiffer gels with mismatched mechanical properties and can hamper basic cell functions such as cell spreading, proliferation and motility.[68] This results in tremendous reduction in the number of "bioinks available", with other most bioinks requiring extensive trade-off in either printability or biocompatibility. Biomaterials are often selected to synthesize bioinks based on their ability to form a structurally stable 3D network under prolonged culture conditions. The formation of such 3D networks can be achieved either via reversible physical or irreversible chemical crosslinking reactions. In the

present day, polymer hydrogels are the most widely used class of bioinks for extrusion based printing due to its above mentioned properties.

For bioprinting applications, hydrogels can be synthesized from either natural polymers such as Gelatin, alginate, and chitosan or synthetic polymers such as poly(N-isopropylacrylamide) (PNIPAm), and polyethylene glycol (PEG). These polymers and their blends can be tailored to be crosslinked to fabricate bio-constructs that possess a wide range of viscoelastic strength, structural stability, and mechanical properties. Crosslinking reactions are known to increase mechanical strength but also hinder printability while affecting bioactivity. Chemical functional groups such as the methacrylate can be added to gelatin, hyaluronic acid and poly(hydroxymethylglycolide-co-ε-caprolactone) to impart mechanical strength and photopolymerizable characteristics.[69, 70] The intensity and duration of UV exposure can be exploited to tailor the matrix stiffness and hydrogel swelling, with higher intensities and longer exposures leading to more crosslinking and thereby producing stiffer constructs. Printability of the construct is dependent on the elastic modulus, viscoelasticity and shear thinning behavior of the bioink. A general strategy to improve printability includes increasing viscosity and decreasing gelation time. Shear thinning implies reduced viscosity with increased shear stress, has the property of decreasing chain entanglement for facile extrusion. Viscosity of the materials is modified by optimization of polymer concentration and density. PCL and PVA increase viscosity aiding extrusion and thus aiding formation of stable printed structures. Filler materials such as nanocellulose, hydroxyapatite, methylcellulose is added to improve shape fidelity and shear thinning. Gelation of the bioink is controlled by careful tuning of the concentration of the polymer and the crosslinking agent. Thermoresponsive polymers when added to the polymer

blend rapidly, and gel upon contact with the print bed providing structural support, hence allowing the requisite time for solidification of the other polymers. This optimization scheme was deployed by Wöst et al, who blended three different materials (gelatin, hyaluronic acid, alginate) for enhancement of mechanical stability throughout the printing process.[71] Individual strengths of polymers were leveraged (hyaluronic acid - viscosity, gelatin - thermal setting, alginate - crosslinking) to produce functional constructs for bone tissue regeneration applications.

Systems to standardize bioink printability by evaluating rheological parameters have been proposed extensively. However, post printing, biocompatibility and bioactivity benchmarks of printed constructs are application specific and are not easy to generalize. While researchers can often fine tune the rheological properties of the bioink by reviewing previously published printability standards, any alteration in terms of chemical crosslinkers, rheological modifiers, or cell densities must be verified to be non-cytotoxic. A general emphasis is placed on maintenance of cellular health and phenotype through appropriate diffusion of nutrients and biochemical stimuli. There still exists a need to evaluate biological performance of different bioinks through pre-screening in order to select an optimal formulation for the bioprinting application. Measures need to be taken towards standardization of the bioprinting process.

Clinical Significance

Need for a 3D patient specific vascularized GBM model

Glioblastoma is the most lethal form of brain cancer with a median survival rate of 12 to 15 months. This low survival rate has been attributed to rapid invasion, cancer stemness, and high therapeutic resistance, all of which have been proven to be controlled by the surrounding tumor microenvironment with GSCs being a key player. The current *in vitro* 3D tumor models and *in vivo* animal models do not capture the pathophysiological features of GBM tumor and are known to impair the treatment process. Specifically, previous models of GBM which include 2D TCPS, organoids, and xenografts are inherently limited and only capture partial characteristics of native GBM.[72] They are either limited to flat morphology, inaccurate architecture, complex but inexact biology (murine models), and/or lack of ECM, tumor microenvironment, tumor heterogeneity, vasculature, and stromal cells. Finally, models for investigating the angiogenesis activity of endothelial cells and GBM cell responses to vascularization are sparse. Thus, there is a strong need for clinically relevant GBM tumor models that can not only capture the complexity of the primary heterogeneous tumor but also be amenable towards detailed pathophysiological investigation.

When developing a novel biomimetic tumor model, there are various factors in design criteria that need to be considered. Although, adding to the complexity of the model (vasculature and stromal/immune cell components) will enhance its relevance and predictive potential, it will also affect its large-scale applications. Hence, in order to be widely accepted in academia and

industry, these models must be simple, yield precise and reproducible outcomes, and standardizable for high throughput applications. In an attempt to capture the heterogeneity and key microenvironment features of the native GBM tumor, we have employed multiple strategies towards our goal of fabricating a simple but holistic GBM model. The incorporation of glycosaminoglycans (GAGs) in the bioink to mimic the ECM of brain tissue is one such strategy. As discussed earlier, in GBM, a vast array of GAGs are known to regulate cell-microenvironment interactions and facilitate diverse functions in the tumor microenvironment. We hypothesized that the presence of GAGs in our 3D bioprinted construct will preserve the stemness and invasive phenotype of the tumor. In addition, we have also created a perivascular niche by printing a hollow encapsulated channel that is lined with ECs. We hypothesized that this niche would allow the preservation of self-renewal properties of GSCs and ensure their sustained proliferation, thereby enhancing its therapeutic resistance, just like the native GBM tumor.

CHAPTER II

MATERIALS AND METHODS

Materials synthesis

Gelatin methacrylate (GelMA) was synthesized by dissolving 10 g of gelatin (Bloom No. 300, Type A, Sigma Aldrich) in 100 ml of 1X PBS (Corning), followed by heating at 60°C for 1 hr. After the gelatin dissolves, 8 ml of methacrylic anhydride was added dropwise and the solution was kept at 60°C for 3 hr. After 3 hr of reaction, 400 ml of preheated 1X PBS was added and allowed to sit for 15 min at 60°C in stirring condition. The solution was then filtered and dialyzed at 50°C for 7 days with change of water 2-3 times each day. After dialysis, GelMA was filtered out, frozen at -80°C for 24 hr and lyophilized for 5-7 days. Lyophilized GelMA samples were stored at -20°C until use.

Chondroitin sulfate methacrylate (CSMA) was synthesized by dissolving 1 g of chondroitin sulfate (Type A, Sigma Aldrich) in 100 ml of MES buffer. For preparing 500 ml of 50 mM MES/0.5 M NaCl buffer solution (pH 6.5), 4.88 g of MES powder was dissolved in 450 ml of DI water. 14.61 g of NaCl was added to the solution and allowed to dissolve in stirring condition. The pH was adjusted to 6.5 using 1N NaOH and/or 1N HCl. Using measuring cylinder, enough DI water was added to obtain a 500 ml solution. After the CS powder dissolves completely and the solution appears clear, 0.27g of NHS (28.5 mM) and 0.85g of EDC (45.6 mM) were added. The reaction between CS and EDC/NHS was allowed to complete for 5 min at room temperature with mild stirring. Then, 0.38g of 2-aminoethyl methacrylate (AEMA) (28.5

mM) was added to the solution and mildly stirred for 24 hr. After 24 hr, the solution was filtered and transferred into a dialysis tube (MWCO = 3500 Da) and dialyzed at room temperature for 3 days. Water was changed 2-3 times per day. After 3 days, the solution was collected in 50 ml centrifuge tubes and store at -80°C overnight. The solution was then lyophilized for 3-5 days. Lyophilized CSMA samples were stored at -20°C until use.

The organoid bioinks were obtained by dissolving the desired w/v concentrations of individual components i.e. GelMA, CSMA, gelatin (Bloom No. 300, Type A, Sigma Aldrich) and irgacure (Sigma Aldrich) in 1X PBS. The solution was interchangeably vortexed and incubated at 40°C for 30-45 min until a homogeneous dispersion was obtained. When necessary, the bioink was covalently cross-linked via exposure to 15 mW/cm^2 365 nm UV light for 60 s. The sacrificial bioink was obtained by dissolving the desired w/v concentration of gelatin in appropriate volume of 1X PBS. The solution was interchangeably vortexed and incubated at 40°C for 30-45 min until a homogeneous dispersion was obtained.

Rheological and mechanical characterization

Rheological characterization was performed using a Discovery Hybrid Rheometer 2 (DHR-2) (TA Instruments), by following the published protocol from our group.[73, 74] A 20 mm parallel plate at gap height of 0.3 mm was used for all experiments unless noted otherwise. Shear rate sweeps, strain sweeps, and peak-hold tests were performed on all polymer precursor solutions to characterize their rheological properties. Shear rate sweeps were carried out sequentially to measure viscosity under a range of shear rate that corresponds to the 3D printing

conditions. Shear rates from 0.01 to 1000 s^{-1} were tested and corresponding viscosity values were noted. The strain sweep was performed at a range of oscillatory strain from 0.1 to 1000 Pa at a frequency of 1 Hz. For the peak hold tests, the shear rate was initially kept constant at 0.75 s^{-1} for 60 sec, then increased to 2000 s^{-1} for 5 sec, and finally dropped to 0.2 s^{-1} for 180 sec. The corresponding changes in viscosity were recorded, and analyzed. These sequential changes in shear rate conditions were representative of the bioink in the extruder, extrusion from the printing nozzle and recovery post extrusion respectively.

Mechanical characterization was performed using an ADMET eXpert 7600 system (ADMET, Inc., Norwood, Massachusetts) with an attached load cell of 25 lb. The testing was performed at a stain rate of 1 mm/min on cylindrical hydrogel samples (~6mm x 1.5mm) through an unconstrained single cycle compression test, in which the crosslinked hydrogels were compressed to 30% of their original height over 1 min, and allowed to revert back over another 1 min. The position and corresponding force data was recorded by the machine, and the compressive modulus, maximum stress and toughness was calculated corresponding to the 10-20% strain region of the engineering stress-strain curve.

Culture media formulations

Serum-free culture media for growing/expanding GSCs

The completed growth media to culture GSCs was made by mixing the following individual components in desired concentrations followed by filter sterilization.

- Neurobasal-A without phenol red (Cat #12349015): 500 ml
- Sodium pyruvate (1% from 100mM stock): 5 ml
- GlutaMAX supplement (1%; Cat #35050061): 5 ml
- Penicillin/Streptomycin (1% from 10,000 U/ml stock): 5 ml
- hEGF: 20 ng/ml in total media
- hFGF: 20 ng/ml in total media
- B27 (2x from 50x stock; Cat #12587010): 10 ml

It is important to note that B27 is relatively unstable upon diluting and continuous exposure to light. Therefore, it is recommended to prepare semi-complete media with all other supplements. For each week's use, 49 ml of media was aliquoted into a 50 mL centrifuge tube and 1 ml of B27 was thawed and added to make complete media.

Serum-free GSC/HUVECs co-culture media

This media was used for assessing co-culture condition that requires the maintenance of GSC stemness. Since the patient-derived GSCs are very sensitive to serum, it was observed that even with 1% serum, the stemness decreases significantly and they start to lose the ability to form neurospheres. On the other hand, culturing ECs in serum free neurobasal media results in round morphology, clumping, and cell death. Thus, this formula of media was designed for the co-culture of both GSCs and HUVECs under serum-free condition. For this formula, Endothelial

Growth Medium Kit (PromoCell Cat#C-22110) was used and the following individual supplements were added in the desired concentrations.

- Endothelial Growth Basal Medium: 50 ml
- 2x of B27 stock: 1 ml
- 1% GlutaMAX: 0.5 ml
- 1% penicillin/streptomycin: 0.5 ml
- 0.1% hydroxycortisone (50 µg/ml total): 0.05 ml
- 0.4% endothelial cell growth supplement (ECGS): 0.2 ml
- 0.5 ng/ml vascular endothelial growth factor (VEGF): 2.5 µl from 10 µg/ml stock
- 20 ng/ml hEGF
- 20 ng/ml hFGF

Growing GSCs in culture flasks

Patient derived GSCs were acquired from Dr. Jeremy Rich's research group by the courtesy of our collaborator, Dr. Irtisha Singh, who has worked with these cells extensively in the past.[75] These cells were derived from surgically resected patient tissues at the Case Western Reserve University with appropriate informed consent and approval from the Cleveland Clinic Institutional Review Board. GSCs were already transduced through lentiviral infection for the constitutive expression of GFP.[13]

The first step towards culturing GSCs in 2D TCPS was to coat the culture flasks with 2% Matrigel. For this, Matrigel® hESC-Qualified Matrix (Cat #354277) was aliquoted in several microcentrifuge tubes (~800 µl/tube) and stored at -20°C to avoid multiple freeze thaw cycles. A 2% Matrigel solution was prepared by adding 800 µl of stock Matrigel solution into 40 ml ice-cold sterile 1X PBS and mixed thoroughly. This solution was used up to 2X to coat culture flasks. The culture flasks were coated by adding 10 ml in T175 flask, 5 ml in T75 flask, and 2 ml in T25 flask, of the 2% Matrigel solution and incubating them at 37°C for 30 min. After incubation, the Matrigel solution was collected back and culture flasks were rinsed once with sterile 1X PBS. The vessels were then considered ready for GSCs culture.

The second step was culturing GSCs in the Matrigel coated culture flasks. GSCs were collected from cryopreservation vials along with 4 ml of growth media into a 15 ml tube. The tube was then centrifuged at 1000 rpm for 5 min and the supernatant was removed. The cell pellet was resuspended with required volume of growth media for each culture vessel, i.e. 5 ml for T25, 10 ml for T75 and 20 ml for T175 flasks. The resuspended cell solution was then added into the coated vessel and cultured at 37°C, and 5% CO_2. Media change was performed every 2 days.

Growing GSC Spheroids

Using inert-grade U-bottom 96-well plates

GSCs were placed as single cells suspension along with 100 µl of growth media at density of 10,000 cells/well into each well of an inert-grade 96-well plate (BRAND Cat#781900). The plate was then centrifuged at 100g (Eppendorf) for 5 min and placed on a shaker and cultured at 37ºC, and 5% CO_2 for 1-2 days. Typically, spheroids formed overnight and reached mature round shape within 2 days under shaking condition. The average spheroid size was calculated to be 200-300 µm.

Using AggreWell™ 400 microwell culture plate

AggreWell400 (Stemcell© Cat#34425) plate was coated with Anti-Adherence Rising Solution (Cat #07010) at 2 ml/well for 6-well AggreWell 400 plate and centrifuged at 1300g (Eppendorf) for 3 min. The plates were checked under a light microscope to ensure there were no bubbles in each microwell. If bubbles were found, the centrifugation step was repeated. The wells were then rinsed with warm sterile 1X PBS. Single GSCs cells suspension were placed in the wells along with 2 ml of growth media at density of 1.5 x 10^6 cells/well (for the 6-well plate type). This seeding density yields spheroids with ~2000 cells/spheroid. The plate was centrifuged at 100g for 5 min and then put for culture at 37°C, and 5% CO_2 for 2 days.

Growing HUVECs in culture flasks

The completed growth media to culture HUVECs was made by mixing 500 ml bottle of Basal Medium (PromoCell) and 5 ml of SupplementMix. HUVECs were collected from cryopreservation vials along with 4 ml of growth media into a 15 ml tube. The tube was then centrifuged at 1000 rpm for 5 min and the supernatant was removed. The cell pellet was resuspended with required volume of growth media for each culture vessel, i.e. 5 ml for T25, 10 ml for T75 and 20 ml for T175 flasks. The resuspended cell solution was then added into the coated vessel and cultured at 37°C, and 5% CO_2. Media change was performed every 2 days.

3D Bioprinting

A commercial ANET A8 3D printer kit was modified to create our custom 3D bioprinter, which utilizes screw-based extrusion. The thermoplastic extruder assembly was substituted with a 3D printed screw extruder assembly, with the addition of a stepper motor, a guide rail, and a modified clay extruder. The first step towards 3D bioprinting was to design the shape to be printed in Solidworks and export them as STL files. Then, Slic3r software was used to “slice” the STL files, which simply means to customize the printing settings and converting them to instructional G-code for the bioprinter. The printing speed was set to 3 mm/s, layer height and extrusion width were kept at 200 um and 0.6 mm, whereas the extrusion multiplier was set to 4 for all trials.

Patient-derived GSCs were cultured in serum-free completed neurobasal medium as mentioned above. GBM organoids were formed by culturing GSCs in ultra-low bind AggreWell™ 400 plates at a density of 2000 cells/microwell for 2 days by following the described protocol. These organoids were then mixed uniformly with the various shear-thinning bioink formulations listed in Table 1 and considered ready for printing. Meanwhile, the sacrificial ink, composed of 4% gelatin, was also prepared and stored at 37°C. The bioink and sacrificial bioink were loaded into two extrusion tubes with a 400 μm non-tapering nozzle tip and extrusion printed through the ANET printer in a sequential manner explained below.

The fabrication of the entire 3D GBM construct with sacrificial channel network was achieved in 3 steps. Step 1: The first layer of the solid cuboidal structure (1.5 cm length, 1.5 cm breadth, and 2 mm height) was 3D printed using the optimal brain-specific bioink with incorporated GBM organoids. Step 2: After gelation using UV crosslinking (15 mW/cm^2 365 nm UV light for 60 sec), the sacrificial bioink was printed in the form of a cylinder (1.5 cm length, 1 mm diameter) on the top of the first cured hydrogel layer. Step 3: Another identical layer of the brain-specific bioink was printed on top, to encapsulate this printed sacrificial channel with similar protocol to the first step. After gelation, the construct was incubated at 37°C, and 5% CO_2 for 30-45 min to allow for the gelatin to melt completely and form a hollow channel. The channel was then flushed with completed Endothelial Growth Media 2 (EGM2) twice to wash off the gelatin. The overall schematic of the bioprinting process has been illustrated in Fig.1.

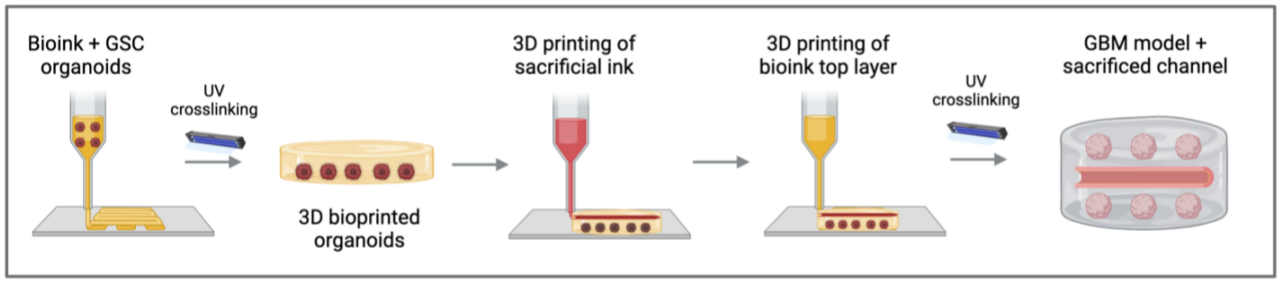

Figure 1: Overall schematic of the bioprinting process

Endothelialization of vascular network

After the organoids and the vascular channel were printed and sacrificed leading to the formation of a hollow channel, 20 µl of HUVECs at a density of $10x10^6$ cells/ml in suspension EGM2 media were seeded into each of the two channel openings with the help of micropipettes. The constructs were then incubated at 37ºC to allow the cells to adhere to the inside of the channel. The construct was then flipped over for the formation of a circumferential confluent lumen. Finally, the constructs are either incubated at 37ºC in static culture or perfusion culture after overnight static incubation at 37ºC. For active perfusion, after the HUVECs have been incubated at 37ºC overnight post seeding, a silicon tube (diameter 1.5 mm) is connected to an 18 gauge needle (inner diameter 0.84 mm) at one end and a peristaltic pump on the other. The other end of the 18 gauge needle is connected to the hollow channel. The entire setup can be visualized in Fig. 6. The perfusion rate was maintained at 10 µl/min.

Immunofluorescence staining

For immunofluorescence, bioprinted constructs were first washed with 1X PBS and then fixed with 4% paraformaldehyde for 15 min. Samples were then permeabilized with 0.2% Triton X for 5 min followed by two washes with 1X PBS. Samples were blocked with 1% bovine serum albumin (BSA) for 45 min and then incubated with primary antibodies overnight at 4°C. The primary antibodies were diluted in blocking buffer (0.5% BSA in PBS containing 0.1% Triton X-100) at a dilution of 1:200. Unbound primary antibodies were removed by washing the constructs with 1X PBS in shaking condition for three times. Samples were then incubated with Cy3 conjugated secondary antibodies for 45 min at 25°C. Then, after two washes with 1X PBS, nuclei were counter-stained with DAPI for 20 min. The samples were then imaged using an epi-fluorescence microscope (Zeiss) or a laser scanning confocal microscope (Lionheart). The images were background corrected using their corresponding negative controls using Image J software.

Analysis of cell viability

Cell viability post printing was determined by staining the bioprinted organoids with 4 μM 'live" calcein AM (Invitrogen) and 2 μM of "dead" ethidium bromide (Invitrogen) for 30 min. Live cells were exhibited green fluorescence by calcein AM (ex/em ~ 495 nm/515 nm), and dead cells showed red fluorescence by ethidium bromide (ex/em ~ 540 nm/615 nm). Cell survival was observed a laser scanning confocal microscope (Lionheart) and live and dead cell quantification was performed by analyzing the corresponding intensity using ImageJ software.

Briefly, after splitting the red and green channels in the RGB image, the area, mean gray value, and standard deviation were obtained by selecting the region of interest (ROI), i.e. organoids. The image acquisition settings and exposure times were kept constant for all samples.

Analysis of cell metabolic activity

Cellular metabolic activity was assessed using the Alamar Blue assay. The stock Alamar Blue solution was diluted 1:10 in warm culture medium. Then, the cell culture media was replaced by the working Alamar Blue solution and incubated at 37ºC for 3 hr. After incubation, 100 µl/well of the media with Alamar Blue solution was collected from each well and transferred to an optical 96-well plate for measuring the fluorescence intensity at excitation 560 nm and emission 590 nm using a TECAN plate reader. Only media was used as blank and four technical replicates were tested for each sample.

RNA Isolation and Quantitative-Reverse-Transcription PCR

RNA was isolated from GBM neurospheres after 7 days using the Quick-RNA MiniPrep kit (Zymogen) by following the manufacturer's instructions. Briefly, the samples were lysed in appropriate volume of RNA lysis buffer. Then, the supernatant was centrifuged in multiple columns, washed with the provided RNA wash buffer, and eluted in 50 µL of RNase/DNA-free water. Cells grown in TCPS dishes for up to 70% confluence were used as 2D controls, and the RNA was isolated as discussed previously. 0.5−2 µg of RNA was used for cDNA synthesis. The samples were first subjected to 2 U/µL DNase in order to remove all traces of genomic DNA.

cDNA synthesis was carried out by using the cDNA qScript SuperMix (Quanta Biosciences) as per the manufacturer's instructions. Quantitative real-time PCR (qRT-PCR) was done using a PowerTrack SYBR green qPCR Kit (Applied Biosystems) with 10 ng of the cDNA as the template. Fold change was calculated. A two-way ANOVA was performed, and $p < 0.05$ was taken as statistically significant.

CHAPTER III

RESULTS AND DISCUSSION

Rheological characterization

The first step of bioprinting, especially with extrusion-based systems, is to ensure that the bioink is printable and optimized for good print fidelity. For this purpose, the bioink must be shear-thinning, i.e. it should exhibit non-Newtonian behavior, characterized by a decrease in viscosity ($n<100$ Pa.s) under shear stress and a recovery when the stress is removed. This behavior is believed to be a consequence of small structural rearrangements within the fluid during shearing. Specifically, in polymer solutions like our bioink, shear thinning is believed to be caused by the disentanglement of anisotropic polymer chains to align in the direction of shear.[76] This leads to a decrease in interaction between smaller units and an increase in free space, thus decreasing viscosity. So, in theory and practice, a shear thinning bioink would show a drop in viscosity when it flows through the extruder tip, but recuperate immediately when shear stress is withdrawn, so as to hold in place and support subsequent top layers.

Gelatin methacrylate or GelMA has been used widely for biomedical applications such as tissue engineering and 3D modeling of cancer.[77, 78] This polymer which has been functionalized with methacrylate groups, forms covalently cross-linked hydrogels when exposed to UV radiation, in the presence of a photoinitiator. Researchers have published several reports affirming the promising features of GelMA as bioinks to fabricate complex 3D geometries for bioprinting applications.[79, 80] Besides being low-cost and abundant, it is hydrolyzed from

collagen, which imparts this polymer with excellent biocompatibility and cell adhesion properties. Chondroitin sulfate on the other hand, represents a major class of GAGs, which has been implicated to play pivotal role during neuronal development, nerve plasticity, formation of PNNs and tissue damage repair.[26] For these reasons, GelMA and CSMA were chosen to be the base components of our bioink formulations. 2% gelatin was added to all bioink formulations to facilitate further gelation of the bioprinted constructs in order to maintain the final shape and structure. 3D printing of two separate layers of bioinks with two subsequent chemical crosslinking steps using UV radiation creates an interface between these layers. This lack of crosslinking between the two layers of bioink demanded the addition of gelatin to prevent their separation on prolonged culture.

In order to print 3D scaffolds with good fidelity and reproducibility, the optimal printing parameters were obtained by evaluating the printability of GelMA/CSMA/gelatin bioinks by

Bioink Formulation	GelMA Conc. (w/v)	CSMA Conc. (w/v)	Gelatin Conc. (w/v)	Irgacure Conc. (w/v)
1	5%	1%	2%	0.01%
2	5%	3%	2%	0.01%
3	7%	1%	2%	0.01%
4	7%	3%	2%	0.01%
5	10%	1%	2%	0.01%
6	10%	3%	2%	0.01%

Table 1: Different formulations of bioink tested with varying concentrations of GelMA, and CSMA.

varying their concentrations, as listed in Table 1. Qualitatively, the printability was assessed by observing (1) if the composition could reach at least 3 mm in height, (2) there are no major defects in the printed construct, and (3) there is negligible patterning in the final construct to signify the lack of "dragging" while printing. Quantitatively, the printability was evaluated by performing rheological characterization of different formulations as shown in Table 1. Fig. 2A presents the change in viscosity of different bioink formulations as a function of shear rate. As it is seen here, shear thinning behavior was confirmed for all bioinks with varying GelMA and CSMA concentrations i.e. the viscosity decreases with increase in shear rate. However, the shear thinning behavior was slightly better for bioinks with higher concentration of GelMA (10% GelMA, 3% CSMA and 10% GelMA, 1% CSMA) than the lower concentration ones (5% GelMA, 3% CSMA and 5% GelMA, 1% CSMA). Peak hold test was done to simulate the three phases that the bioink encounters during the printing process: a pre-extrusion phase, extrusion phase, and a post extrusion phase (Fig. 2C). The pre-extrusion phase features a low shear rate (0.75 s^{-1}) which represents the shear condition in the extruder barrel. Then, this was followed by an increase in shear rate (2000 s^{-1}) for 5 seconds to simulate extrusion through the extruder nozzle/tip. The bioink was then held at a low shear rate (0.25 s^{-1}) to simulate the shear condition post printing. An ideal printable bioink should show a rapid drop in viscosity during the high-shear extrusion phase and then, a rapid recovery within seconds post extrusion. As seen in Fig. 2C, all the bioink formulations that were tested showed this behavior but with different recoveries in viscosity, which have been calculated in Table 2. The percentage recoveries were calculated by dividing the final viscosity post extrusion phase with the initial viscosity pre extrusion phase and then multiplying it by 100. According to viscosity recovery data from peak hold tests, 7% GelMA, 1% CSMA is the bioink formulation that has the best printability due to

highest recovery (~51%) in viscosity. The next best recovery in viscosity (22.4%) was shown by 7% GelMA with 3% CSMA indicating slightly better shear thinning properties relative to other formulations. The bioink formulations with highest GelMA concentration, i.e. 10% GelMA, 1% CSMA and 10% GelMA and 3% CSMA showed 12.2% and 15.6% recovery in viscosity respectively. Moreover, when both these formulations were printed, cell shearing was observed with single cells dislodging from the organoids. Also, the organoid morphology was compromised (Fig. 2F), i.e. organoids were slightly elongated and elliptical as opposed to their usual spherical shape as seen in Fig. 4. This observation was not unusual since past studies have

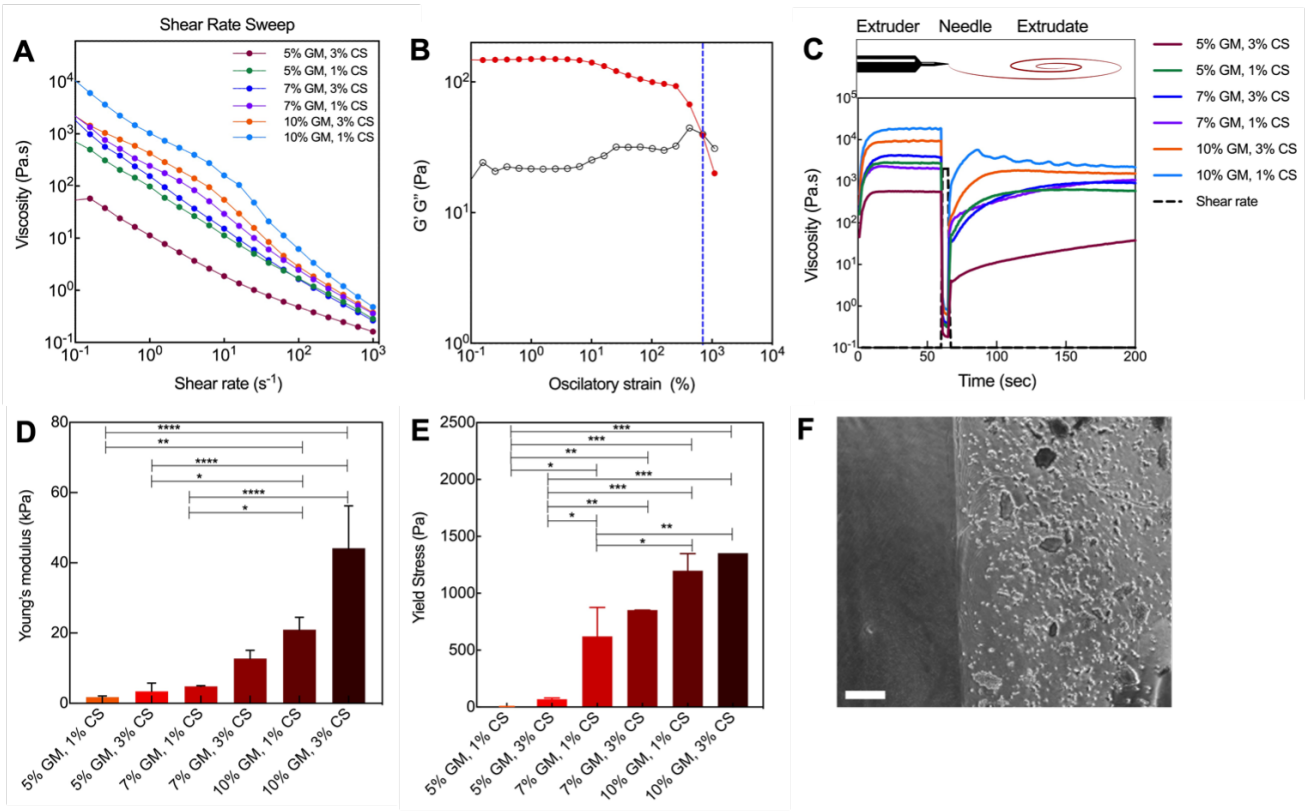

Figure 2: Rheological characterization of GelMA and CSMA bioink formulations. (A) Shear rate sweep; (B) Strain sweeps; (C) Peak hold experiments to mimic flow during extrusion/printing; (D) Young's compression modulus; (E) Yield stress quantification; (F) Phase contrast image shows cell shearing post-printing. Scale bar 200 µm.

shown that low-concentration GelMA hydrogels are better suited for 3D printed cell laden constructs due to enhanced cell stability and viability.[81] Therefore, both these formulations were deemed unfit for our application. Due to these reasons, and based on rheological properties and printability, the bioink composition of 7% GelMA with 1% CSMA was the ideal candidate for printing GSC organoids and functional studies.

Bioink Formulation	GelMA Conc. (w/v)	CSMA Conc. (w/v)	Initial Viscosity (Pa.s)	Final Viscosity (Pa.s)	Recovery (%)= (Final/Initial) x100
1	5%	1%	2761.01	584.91	21.2%
2	5%	3%	570.92	37.62	6.6%
3	7%	1%	2086.70	1061.50	50.9%
4	7%	3%	4053.60	908.43	22.4%
5	10%	1%	18131.0	2208.40	12.2%
6	10%	3%	9738.0	1521.0	15.6%

Table 2: Percentage recovery in viscocity for different formulations of bioink tested.

Mechanical properties

The mechanical properties of the tumor microenvironment are known to regulate the behavior of GBM tumor. To elicit similar mechanical cues *ex vivo*, controlling the mechanical properties of 3D printed constructs becomes crucial. Keeping this in mind, we aimed for our 3D printed constructs to have comparable mechanical properties as the GBM tissue. For this purpose, we investigated the mechanical properties of the crosslinked bioink formulations at 25ºC. Unconfined compression tests were performed to characterize the bioinks' mechanical

properties. Young's modulus, which was derived from the stress-strain curves for all bioink formulations, has been plotted in Fig. 2D. Not surprisingly, the stiffness of the GelMA/CSMA hydrogels was directly proportional to an increase in their respective concentrations. We found that 10% GelMA, 3% CSMA hydrogels showed a much higher compressive modulus (44.5 kPa), nearly ten times more, as compared to 5% GelMA, 1% CSMA samples. After eliminating 10% GelMA bioink formulations due to cell shearing, the next best candidate that shows optimal mechanomimetic properties with good print fidelity is 7% GelMA, 1% CSMA. GBM tumors have been reported to exhibit a wide range of elastic modulus from 0.1 kPa in necrotic regions to up to 10 kPa in hypercellular region.[53] The elastic modulus of the 7% GelMA, 1% CSMA was calculated to be 4.80 kPa (Fig. 2D), which is significantly lesser than that of standard TCPS dishes (2.79 GPa) and similar to that of GBM tumors (0.1-10 kPa). Since mechanical properties of the tumor microenvironment play a key role in affecting cell behavior *in vivo*, the bioprinted mechano-mimetic constructs were expected to provide a conducive environment for cell growth.

Multipotency of GSC organoids

GSCs are typically distinguished within a tumor cell population by their stemness, multipotency and self-renewal properties. Multipotent GSCs play a central role in the aggressiveness and therapeutic evasion of GBM. Their ability to give rise to multiple cell types in the tumor stroma (e.g. pericytes, astrocytes, ECs) enables survival of glioblastomas through therapeutic stress and contributes to tumor relapse. Recapitulating this trace by incorporating GSCs into 3D bioprinted GBM construct is the first step in the developing of a clinical-relevant GBM model.

Past studies have shown that multiple signalling pathways are upregulated in the perivascular niche, and highlighted the role of endothelial cell derived factors to preserve GSC stemness.[39] Since we are attempting to recreate the perivascular niche, we wanted to gain some insight on the effect of soluble factors secreted by ECs on the stemness and multipotency of GSCs. For this purpose, we cultured GSC neurospheres in a transwell culture system with ECs, only allowing the interaction of secreted soluble factors. This experiment was crucial to ensure and verify the stemness and multipotency of GSCs before bioprinting. The multipotency of GSCs neurospheres was determined by co-culturing them with or without ECs in serum free culture media and then following up with immunofluorescence staining. After 7 days of culture, differentiated GSCs were stained for markers of astrocytic lineage (GFAP), pericytic lineage (CD146), and endothelial cell lineage (CD31). This was done for both groups, group 1 GSCs and group 2 GSCs, and in both groups, GSCs differentiated into other neural cell subtypes indicating that multipotency was preserved and maintained (Fig. 3A). For stemness, we immunostained the GSC neurospheres for nestin either with or without ECs, at day 7. We observed considerable expression of nestin, indicating that GSC stemness was preserved as well (Fig. 3A).

After confirming the preservation of stemness and multipotency of GSCs, we also performed RT-PCR experiments to quantify the expression of these markers: nestin, CD146 and CD31, in similar transwell co-culture experiments. We observed that nestin mRNA levels in the coculture of group 1 GSCs and ECs was slightly higher than the ones without ECs but this difference was not as significant for group 2 (Fig. 3B, 3C). The expression of CD146 was relatively similar in group 1 and group 2 as compared to the corresponding controls. But, not surprisingly, CD31 expression went up in both groups signifying considerable differentiation of

GSCs towards EC lineage (Fig. 3B, 3C). This upregulation CD31 expression in GSC neurospheres indicates the mimicking of *in vivo* GBM tumor microenvironment, where GSCs tend to transdifferentiate to an endothelial cell when required, with regard to the tumor progression.

Apart from this, we also observed a more invasive phenotype in group 1 GSCs with some cells invading out of neurospheres (Fig. 3A). As opposed to this, group 2 GSCs were somewhat

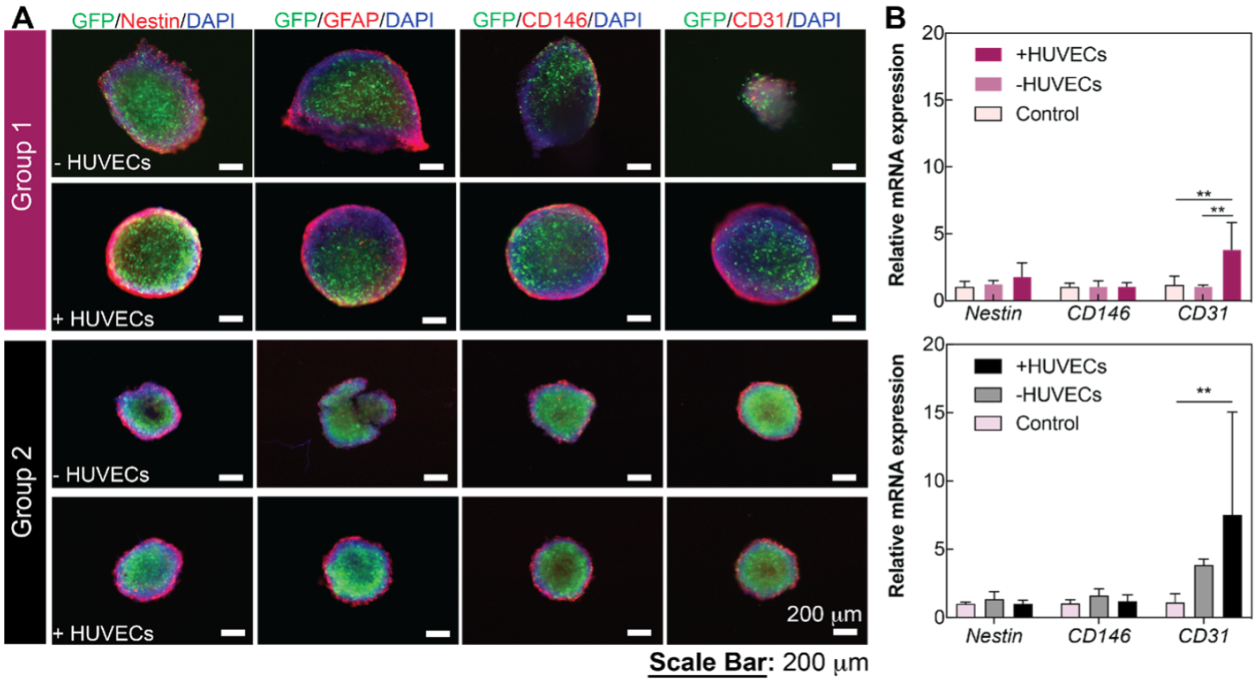

Figure 3: (A) Multipotent characteristics of GBM organoids in the presence or absence of HUVECs. Progenitor cell marker (Nestin), astrocytic marker (GFAP), pericyte marker (CD146), and endothelial marker (CD31) in red, GFP expressing GSCs in green and nucleus in blue; Scale bar: 200 µm. (B) Relative mRNA expression of Nestin, CD146, and CD31 in the presence and absence of HUVECs in Group 1 GSCs. (C) Relative mRNA expression of Nestin, CD146, and CD31 in the presence and absence of HUVECs in Group 2 GSCs. Acknowledgement: Dr. Thuy-Uyen Nguyen.

"dormant" and showed a more constraint morphology. This observation was not unusual since past research on mapping chromatin landscapes of these groups found group 1 to exhibit more "proliferative" and "proneural" features while group 2 showed a "mesenchymal" phenotype.[75] Together, this data suggests that these patient-derived GSCs are able to sustain their stemness and can differentiate when cued. This result also proves our ability to obtain multipotent GBM organoids from patient-derived GSCs for the development of a 3D bioprinted GBM model.

Morphology, cell viability and cell metabolic activity post-printing

One of the bottle necks in the field of extrusion based 3D bioprinting is ensuring that cells are viable and metabolic activity/proliferation is preserved post printing. Cells are under the effect of shear forces during extrusion, and sometimes exposed to unfavorable temperatures and growth conditions during the bioprinting process. Also, the addition of rheological modifiers such as nanoparticles might lead to cellular toxicity and death, as discussed before. However, we did not anticipate a decline in viability due to the lack of rheological modifiers in our bioink. But, we still had to account for the effect of other parameters such as shear stress and degradation products on cell viability. Therefore, we investigated the biocompatibility of 3D bioprinted GSC organoids in the 7% GelMA, 1% CSMA hydrogel by measuring cell viability via staining them with calcein AM (live) and ethidium bromide (dead). The cell viability was also quantified by measuring the intensity of live and dead staining after being background corrected with respective controls. In addition, we performed the Alamar Blue assay to quantify the metabolic activity of these organoids at day 1, 3, 5 and 7.

Results showed that GSC organoids were able to maintain intact spherical morphology (Fig. 4B) and avoided shearing during the printing process. A high survival rate of 95-100 % was observed for both groups of bioprinted GSCs at day 1 and 7 (Fig. 4C). Results from the Alamar Blue assay showed that both groups showed a steady increase in proliferation over the course of 7 days (Fig. 4D). It was also noticeable that group 1 GSCs are more proliferative than group 2 GSCs and this trend grew stronger with each passing day of culture. But, this is not surprising as it is in corroboration of our knowledge of these GSCs groups that group 1 exhibits a more "proliferative" phenotype. Together, this data shows that we were able to 3D print two heterogeneous groups of GSCs with high cell viability, metabolic activity and intact morphology for long term *in vitro* culture.

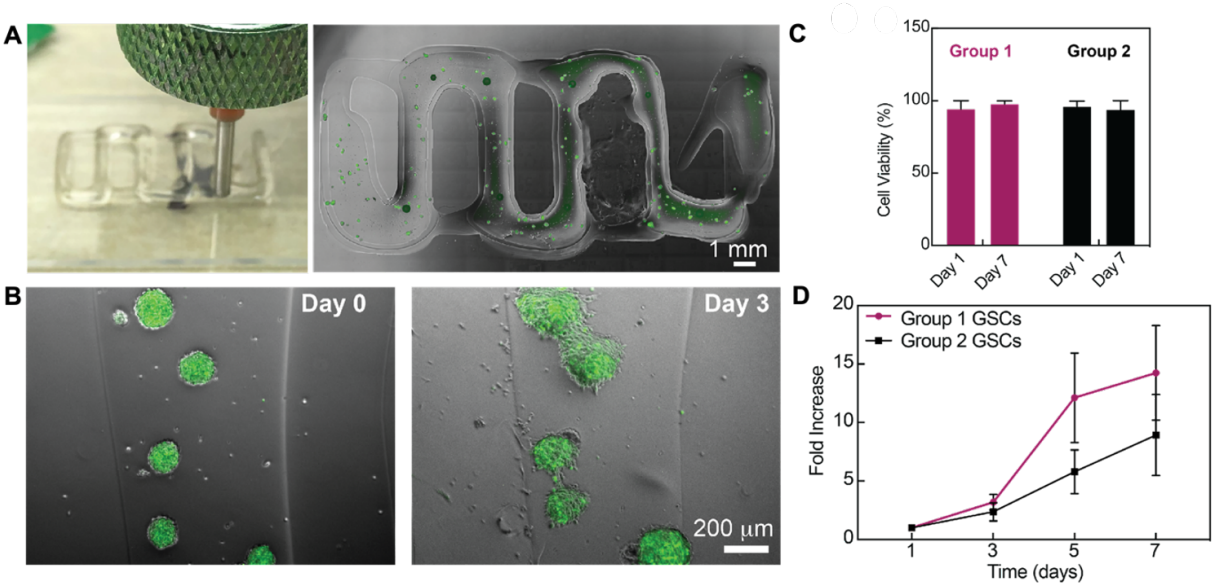

Figure 4: Intact morphology, high cell viability, and high metabolic activity of bioprinted GSCs. (A) 3D bioprinting of GSC spheroids in a serpentine geometry; (B) Presence of GBM organoids within the 3D printed constructs with intact morphology; (C) High cell viability post-printing; (D) Increasing metabolic activity post printing.

Enhanced invasion in bioprinted constructs

After we ensured that our bioprinted constructs were capable of supporting the attachment and proliferation of ECs, and establish a perivascular niche, we wanted to evaluate the effect of ECs on the invasion potential of bioprinted GSCs. It is well known that the GBM tumor microenvironment and the perivascular niche contribute to tumor invasion.[82] Here, we demonstrate the use of our bioengineered GBM model to evaluate the invasion of glioblastoma stem cells towards vasculature and also sprouting angiogenesis. The sprouting of HUVECs as well as the invasion of GSC organoids was monitored through the utilization of GFP expressing GSCs (GFP GSCs). Biological sections of the co-culture system were observed and imaged using a confocal microscope. The distance of GSCs invasion and HUVECs sprouting was determined via ImageJ by setting the initial organoid periphery as the boundary for GSCs and the baseline where HUVECs are in contact with the brain-specific ECM bioink was set as the boundary for HUVECs. As it is seen in Fig. 5C, the distance between GSCs and ECs decreased progressively over 6 days of culture. Interestingly, both cell types were invading the surrounding gel and migrating towards each other (Fig. 5A, 5B). ECs have been reported to exhibit this "sprouting" phenotype under the influence of GSCs via multiple mechanisms.[83] Studies have shown that GSCs release pro-angiogenic factors such as VEGF and SDF-1a to promote angiogenesis. Folkins et al. showed that the microvessel densities were enhanced in tumors rich in GSCs in xenograft models of glioblastoma.[84] They also noted that VEGF and SDF-1a were significantly upregulated in GSC rich tumors and their blockade caused the level of vascularization to decrease. GSCs on the other hand, also infiltrate towards the ECs, which is not surprising considering their predilection to vasculature. This behavior is probably a

preferential response to nutrients and cues from the tumor microenvironment to promote tumor survival. Past studies have shown this preferential behavior of GSCs towards vasculature to be a consequence of chemo-attractive soluble factors in the perivascular niche. For example, Bradykinin (BK) is known to initiate chemotactic signaling in the perivascular niche and facilitate GSC invasion.[85] Future studies will investigate the effect of ECs on the malignancy of GSC organoids by real-time PCR to assess the expression of invasion-associated markers L1CAM, CXCR4, MMP16, integrin α2, and integrin β3. In addition, to verify if the crosstalk between GSCs and ECs is originating from the pro-angiogenic nature of GSCs, the expression of pro-angiogenic markers IL-840-41 and VEGF will also be quantified.

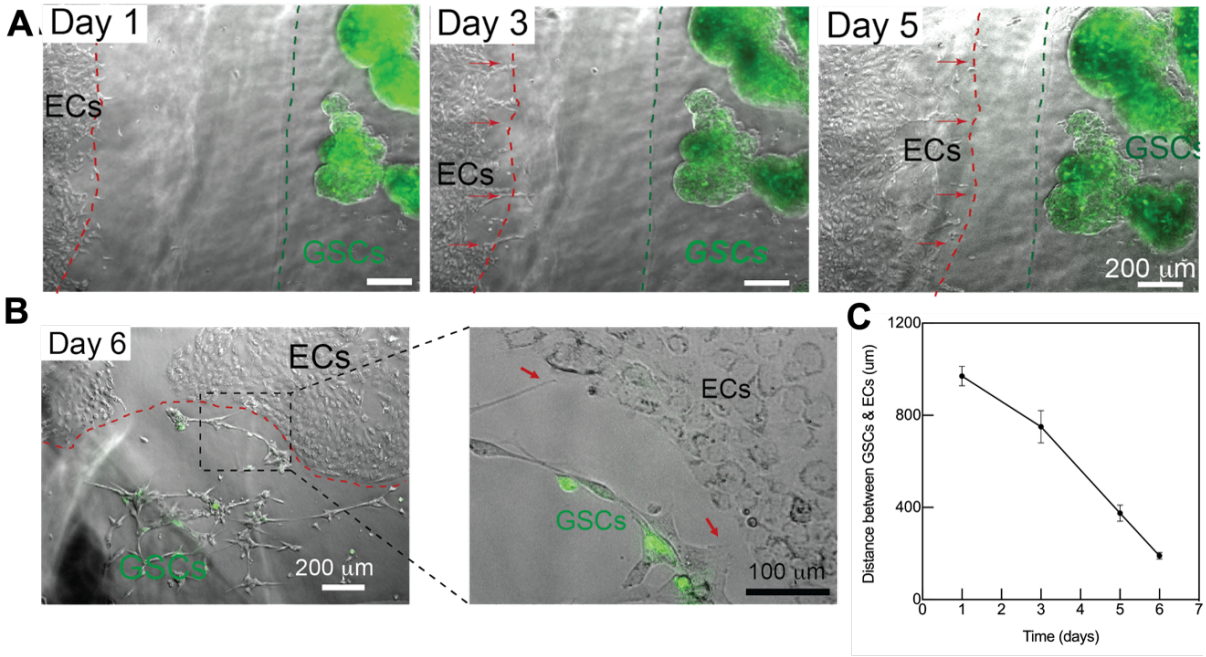

Figure 5: Enhanced invasion in bioprinted constructs. (A) Invasion of GSCs and ECs in 3D bioprinted constructs at say 1, 3 and 5. GSC organoids in green. Scale bar: 200 µm; (B) Interaction between GSCs at ECs was observed at day 6. (C) Quantification of invasion distance.

Perfusion flow

An ideal vascularized tissue construct is typically made of three essential components: the vascular lumen, which acts as a source and sink to exchange soluble factors, and endothelial cells lining this vascular lumen, and a dynamic perfusion flow. The final step towards combining these three crucial factors into our bioengineered model was to introduce perfusion flow into the endothelialized channel. Flow induced shear stresses have a significant impact on the function of GSCs and proliferation of ECs.[86] Therefore, it is imperative that we simulate the appropriate shear stresses in the endothelial lumen to achieve cellular confluency throughout the lumen and also mimic the perivascular niche. The perfusion setup has been shown in Fig. 6A. We used a peristaltic motor to pump nutrient rich media into one inlet and let it out the other into a discard sink in a discontinuous loop. For our experiments, we set the flow rate to be at 10 µl/min, which was inspired by past literature.[87] Kolesky et al. have showed that this flow rate was adequate to generate the appropriate shear force in a vascular channel with dimensions similar to our model.

As our first step, we wanted to standardize the flow rate in our perfusion system for which we chose to do short term perfusion of 48 hr. After 48 hr of perfusion culture, we observed the proliferation of ECs in the vascular channel and the formation of tight junctions, as characterized by VE-cadherin staining (Fig. 6B). Since we did not see significant proliferation, for one of our samples, we continued culturing the ECs in the vascular channel for prolonged duration of 10 days, after 48 hr of perfusion flow, to see if ECs are able to achieve confluency in the lumen. Qualitatively, we did not observe any significant change. Future experiments will be targeted to optimize the flow rate so as to improve EC adhesion to the channel. These results

indicated that although the perfusion culture was conducive for endothelial cell attachment and proliferation, multiple parameters such as flow rate and shear forces need to be optimized to result in a confluent EC lumen on prolonged culture.

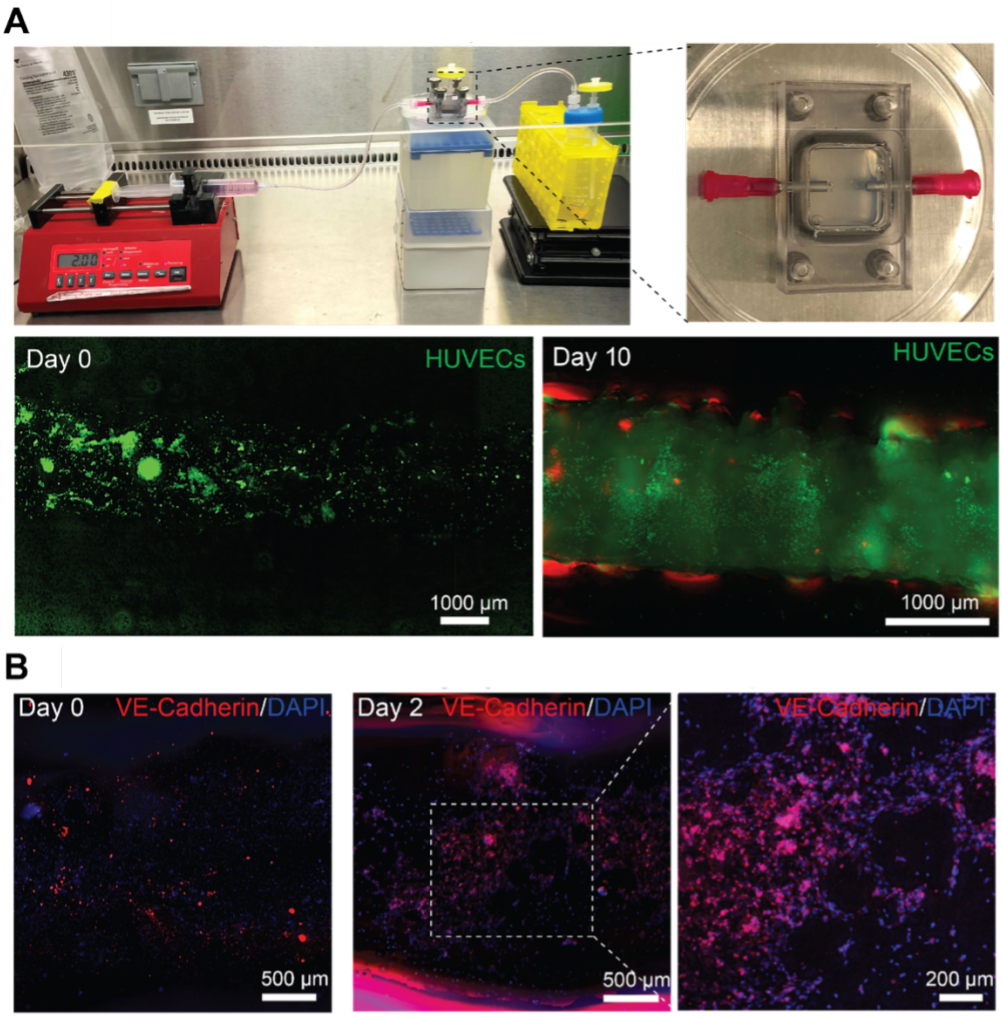

Figure 6: Perfusion flow. (A) Perfusion flow assembly of the 3D printed construct; (B) Immunofluorescence staining for VE-cadherin (red) and nucleus (blue) showed the formation of tight junctions in the channel.

CHAPTER IV

CONCLUSION AND FUTURE WORK

Conclusion

In conclusion, we were able to achieve the aims and objectives of our research. We characterized the different bioink formulations of GelMA and CSMA for better printability and cell viability post printing. We also ensured that the mechanical properties of the bioprinted constructs were comparable to that of GBM tissue. This was achieved by performing multiple rheological tests for quantifying viscosity, shear rate, young's modulus, and yield stress. Then, we were able to 3D print the desired geometries with our optimized bioink formulation of 7% GelMA and 1% CSMA. We proved our ability to obtain multipotent GBM organoids from patient-derived GSCs for bioprinting applications. We were able to 3D print two heterogeneous groups of GSCs with high cell viability, metabolic activity and intact morphology. The sprouting of ECs and the invasion of GSC organoids was reported in the 3D printed constructs. We were also able to achieve perfusion flow through our vascular channel, and that this model could be used to study various pathological features of GBM such as invasion and angiogenesis.

Future work

In future, we will investigate further effects of the tumor microenvironment and optimize the 3D printed perfusable vasculature to gain more insight into the regulation of molecular pathways in our patient specific GBM model.

1. We will utilize a dual-head custom 3D bioprinter to co-print GSC organoids and the vascular channel. This dual-head 3D bioprinter will give us more control over the positioning of GSC organoids and the vascular channel and help us to model different anatomical situations.
2. We will investigate the presence of GSC-derived pericytes and ECs in engineered GBM model by performing lineage tracing of constitutively green-fluorescence-protein (GFP) expressing GSCs. This will highlight the ability of our bioprinted model to induce the differentiation of GSCs into pericytes and ECs.
3. We will optimize the flow rate through the vascular channel so as to generate apt shear forces to improve EC adhesion to the channel.

REFERENCES

1. Gliocure Glioblastoma Facts & Figures. https://www.gliocure.com/en/patients/glioblastoma/ (accessed 10.02.2021).

2. Sung, H.; Ferlay, J.; Siegel, R. L.; Laversanne, M.; Soerjomataram, I.; Jemal, A.; Bray, F., Global Cancer Statistics 2020: GLOBOCAN Estimates of Incidence and Mortality Worldwide for 36 Cancers in 185 Countries. *CA Cancer J Clin* **2021,** *71* (3), 209-249.

3. Stupp, R.; Mason, W. P.; van den Bent, M. J.; Weller, M.; Fisher, B.; Taphoorn, M. J.; Belanger, K.; Brandes, A. A.; Marosi, C.; Bogdahn, U.; Curschmann, J.; Janzer, R. C.; Ludwin, S. K.; Gorlia, T.; Allgeier, A.; Lacombe, D.; Cairncross, J. G.; Eisenhauer, E.; Mirimanoff, R. O.; European Organisation for, R.; Treatment of Cancer Brain, T.; Radiotherapy, G.; National Cancer Institute of Canada Clinical Trials, G., Radiotherapy plus concomitant and adjuvant temozolomide for glioblastoma. *N Engl J Med* **2005,** *352* (10), 987-96.

4. Louis, D. N.; Perry, A.; Reifenberger, G.; von Deimling, A.; Figarella-Branger, D.; Cavenee, W. K.; Ohgaki, H.; Wiestler, O. D.; Kleihues, P.; Ellison, D. W., The 2016 World Health Organization Classification of Tumors of the Central Nervous System: a summary. *Acta Neuropathol* **2016,** *131* (6), 803-20.

5. GLIADEL® Wafer (carmustine implant) for intracranial use [Prescribing Information]. *Atlanta, GA: Arbor Pharmaceuticals, LLC* **August 2018**.

6. Kamb, A.; Wee, S.; Lengauer, C., Opinion - Why is cancer drug discovery so difficult? *Nat Rev Drug Discov* **2007,** *6* (2), 115-120.

7. Gillet, J. P.; Calcagno, A. M.; Varma, S.; Marino, M.; Green, L. J.; Vora, M. I.; Patel, C.; Orina, J. N.; Eliseeva, T. A.; Singal, V.; Padmanabhan, R.; Davidson, B.; Ganapathi, R.;

Sood, A. K.; Rueda, B. R.; Ambudkar, S. V.; Gottesman, M. M., Redefining the relevance of established cancer cell lines to the study of mechanisms of clinical anti-cancer drug resistance. *Proc Natl Acad Sci U S A* **2011,** *108* (46), 18708-13.

8. Tan, B. T.; Park, C. Y.; Ailles, L. E.; Weissman, I. L., The cancer stem cell hypothesis: a work in progress. *Lab Invest* **2006,** *86* (12), 1203-7.

9. Lapidot, T.; Sirard, C.; Vormoor, J.; Murdoch, B.; Hoang, T.; Caceres-cortes, J.; Minden, M.; Paterson, B.; Caligiuri, M. A.; Dick, J. E., A Cell Initiating Human Acute Myeloid-Leukemia after Transplantation into Scid Mice. *Nature* **1994,** *367* (6464), 645-648.

10. Singh, S. K.; Hawkins, C.; Clarke, I. D.; Squire, J. A.; Bayani, J.; Hide, T.; Henkelman, R. M.; Cusimano, M. D.; Dirks, P. B., Identification of human brain tumour initiating cells. *Nature* **2004,** *432* (7015), 396-401.

11. Ligon, K. L.; Huillard, E.; Mehta, S.; Kesari, S.; Liu, H.; Alberta, J. A.; Bachoo, R. M.; Kane, M.; Louis, D. N.; Depinho, R. A.; Anderson, D. J.; Stiles, C. D.; Rowitch, D. H., Olig2-regulated lineage-restricted pathway controls replication competence in neural stem cells and malignant glioma. *Neuron* **2007,** *53* (4), 503-17.

12. Jackson, E. L.; Garcia-Verdugo, J. M.; Gil-Perotin, S.; Roy, M.; Quinones-Hinojosa, A.; VandenBerg, S.; Alvarez-Buylla, A., PDGFRα-Positive B Cells Are Neural Stem Cells in the Adult SVZ that Form Glioma-like Growths in Response to Increased PDGF Signaling. *Neuron* **2006,** *51* (2), 187-199.

13. Cheng, L.; Huang, Z.; Zhou, W.; Wu, Q.; Donnola, S.; Liu, J. K.; Fang, X.; Sloan, A. E.; Mao, Y.; Lathia, J. D.; Min, W.; McLendon, R. E.; Rich, J. N.; Bao, S., Glioblastoma stem cells generate vascular pericytes to support vessel function and tumor growth. *Cell* **2013,** *153* (1), 139-52.

14. Zhou, W.; Ke, S. Q.; Huang, Z.; Flavahan, W.; Fang, X.; Paul, J.; Wu, L.; Sloan, A. E.; McLendon, R. E.; Li, X.; Rich, J. N.; Bao, S., Periostin secreted by glioblastoma stem cells recruits M2 tumour-associated macrophages and promotes malignant growth. *Nat Cell Biol* **2015,** *17* (2), 170-82.

15. Bhaduri, A.; Di Lullo, E.; Jung, D.; Muller, S.; Crouch, E. E.; Espinosa, C. S.; Ozawa, T.; Alvarado, B.; Spatazza, J.; Cadwell, C. R.; Wilkins, G.; Velmeshev, D.; Liu, S. J.; Malatesta, M.; Andrews, M. G.; Mostajo-Radji, M. A.; Huang, E. J.; Nowakowski, T. J.; Lim, D. A.; Diaz, A.; Raleigh, D. R.; Kriegstein, A. R., Outer Radial Glia-like Cancer Stem Cells Contribute to Heterogeneity of Glioblastoma. *Cell Stem Cell* **2020,** *26* (1), 48-63 e6.

16. Prager, B. C.; Bhargava, S.; Mahadev, V.; Hubert, C. G.; Rich, J. N., Glioblastoma Stem cells: Driving Resilience through Chaos. *Trends Cancer* **2020,** *6* (3), 223-235.

17. Negrini, S.; Gorgoulis, V. G.; Halazonetis, T. D., Genomic instability - an evolving hallmark of cancer. *Nat Rev Mol Cell Bio* **2010,** *11* (3), 220-228.

18. Peng, C. H.; Chen, Z. X.; Wang, S.; Wang, H. W.; Qiu, W. J.; Zhao, L.; Xu, R.; Luo, H.; Chen, Y. Y.; Chen, D.; You, Y. P.; Liu, N.; Wang, H. B., The Error-Prone DNA Polymerase kappa Promotes Temozolomide Resistance in Glioblastoma through Rad17-Dependent Activation of ATR-Chk1 Signaling. *Cancer Research* **2016,** *76* (8), 2340-2353.

19. Bao, S. D.; Wu, Q. L.; McLendon, R. E.; Hao, Y. L.; Shi, Q.; Hjelmeland, A. B.; Dewhirst, M. W.; Bigner, D. D.; Rich, J. N., Glioma stem cells promote radioresistance by preferential activation of the DNA damage response. *Nature* **2006,** *444* (7120), 756-760.

20. Wang, J. L.; Wakeman, T. P.; Lathia, J. D.; Hjelmeland, A. B.; Wang, X. F.; White, R. R.; Rich, J. N.; Sullenger, B. A., Notch Promotes Radioresistance of Glioma Stem Cells. *Stem Cells* **2010,** *28* (1), 17-28.

21. Moore, K. A.; Lemischka, I. R., Stem cells and their niches. *Science* **2006,** *311* (5769), 1880-1885.

22. McCord, A. M.; Jamal, M.; Shankavaram, U. T.; Lang, F. F.; Camphausen, K.; Tofilon, P. J., Physiologic oxygen concentration enhances the stem-like properties of CD133+ human glioblastoma cells in vitro (vol 7, pg 489, 2009). *Molecular Cancer Research* **2009,** *7* (6), 987-987.

23. Hjelmeland, A. B.; Wu, Q.; Heddleston, J. M.; Choudhary, G. S.; MacSwords, J.; Lathia, J. D.; McLendon, R.; Lindner, D.; Sloan, A.; Rich, J. N., Acidic stress promotes a glioma stem cell phenotype. *Cell Death Differ* **2011,** *18* (5), 829-840.

24. Charles, N. A.; Holland, E. C.; Gilbertson, R.; Glass, R.; Kettenmann, H., The brain tumor microenvironment. *Glia* **2011,** *59* (8), 1169-80.

25. Schiffer, D.; Annovazzi, L.; Casalone, C.; Corona, C.; Mellai, M., Glioblastoma: Microenvironment and Niche Concept. *Cancers* **2019,** *11* (1).

26. Kwok, J. C.; Warren, P.; Fawcett, J. W., Chondroitin sulfate: a key molecule in the brain matrix. *Int J Biochem Cell Biol* **2012,** *44* (4), 582-6.

27. Munkley, J.; Elliott, D. J., Hallmarks of glycosylation in cancer. *Oncotarget* **2016,** *7* (23), 35478-89.

28. Chin, L.; Meyerson, M.; Aldape, K.; Bigner, D.; Mikkelsen, T.; VandenBerg, S.; Kahn, A.; Penny, R.; Ferguson, M. L.; Gerhard, D. S.; Getz, G.; Brennan, C.; Taylor, B. S.; Winckler, W.; Park, P.; Ladanyi, M.; Hoadley, K. A.; Verhaak, R. G. W.; Hayes, D. N.; Spellman, P. T.; Absher, D.; Weir, B. A.; Ding, L.; Wheeler, D.; Lawrence, M. S.; Cibulskis, K.; Mardis, E.; Zhang, J. H.; Wilson, R. K.; Donehower, L.; Wheeler, D. A.; Purdom, E.; Wallis, J.; Laird, P. W.; Herman, J. G.; Schuebel, K. E.; Weisenberger, D. J.; Baylin, S. B.;

Schultz, N.; Yao, J.; Wiedemeyer, R.; Weinstein, J.; Sander, C.; Gibbs, R. A.; Gray, J.; Kucherlapati, R.; Lander, E. S.; Myers, R. M.; Perou, C. M.; McLendon, R.; Friedman, A.; Van Meir, E. G.; Brat, D. J.; Mastrogianakis, G. M.; Olson, J. J.; Lehman, N.; Yung, W. K. A.; Bogler, O.; Berger, M.; Prados, M.; Muzny, D.; Morgan, M.; Scherer, S.; Sabo, A.; Nazareth, L.; Lewis, L.; Hall, O.; Zhu, Y. M.; Ren, Y. R.; Alvi, O.; Yao, J. Q.; Hawes, A.; Jhangiani, S.; Fowler, G.; San Lucas, A.; Kovar, C.; Cree, A.; Dinh, H.; Santibanez, J.; Joshi, V.; Gonzalez-Garay, M. L.; Miller, C. A.; Milosavljevic, A.; Sougnez, C.; Fennell, T.; Mahan, S.; Wilkinson, J.; Ziaugra, L.; Onofrio, R.; Bloom, T.; Nicol, R.; Ardlie, K.; Baldwin, J.; Gabriel, S.; Fulton, R. S.; McLellan, M. D.; Larson, D. E.; Shi, X. Q.; Abbott, R.; Fulton, L.; Chen, K.; Koboldt, D. C.; Wendl, M. C.; Meyer, R.; Tang, Y. Z.; Lin, L.; Osborne, J. R.; Dunford-Shore, B. H.; Miner, T. L.; Delehaunty, K.; Markovic, C.; Swift, G.; Courtney, W.; Pohl, C.; Abbott, S.; Hawkins, A.; Leong, S.; Haipek, C.; Schmidt, H.; Wiechert, M.; Vickery, T.; Scott, S.; Dooling, D. J.; Chinwalla, A.; Weinstock, G. M.; O'Kelly, M.; Robinson, J.; Alexe, G.; Beroukhim, R.; Carter, S.; Chiang, D.; Gould, J.; Gupta, S.; Korn, J.; Mermel, C.; Mesirov, J.; Monti, S.; Nguyen, H.; Parkin, M.; Reich, M.; Stransky, N.; Garraway, L.; Golub, T.; Protopopov, A.; Perna, I.; Aronson, S.; Sathiamoorthy, N.; Ren, G.; Kim, H.; Kong, S. K.; Xiao, Y. H.; Kohane, I. S.; Seidman, J.; Cope, L.; Pan, F.; Van Den Berg, D.; Van Neste, L.; Yi, J. M.; Li, J. Z.; Southwick, A.; Brady, S.; Aggarwal, A.; Chung, T.; Sherlock, G.; Brooks, J. D.; Jakkula, L. R.; Lapuk, A. V.; Marr, H.; Dorton, S.; Choi, Y. G.; Han, J.; Ray, A.; Wang, V.; Durinck, S.; Robinson, M.; Wang, N. J.; Vranizan, K.; Peng, V.; Van Name, E.; Fontenay, G. V.; Ngai, J.; Conboy, J. G.; Parvin, B.; Feiler, H. S.; Speed, T. P.; Socci, N. D.; Olshen, A.; Lash, A.; Reva, B.; Antipin, Y.; Stukalov, A.; Gross, B.; Cerami, E.; Wang, W. Q.; Qin, L. X.; Seshan, V. E.;

Villafania, L.; Cavatore, M.; Borsu, L.; Viale, A.; Gerald, W.; Topal, M. D.; Qi, Y.; Balu, S.; Shi, Y.; Wu, G.; Bittner, M.; Shelton, T.; Lenkiewicz, E.; Morris, S.; Beasley, D.; Sanders, S.; Sfeir, R.; Chen, J.; Nassau, D.; Feng, L.; Hickey, E.; Schaefer, C.; Madhavan, S.; Buetow, K.; Barker, A.; Vockley, J.; Compton, C.; Vaught, J.; Fielding, P.; Collins, F.; Good, P.; Guyer, M.; Ozenberger, B.; Peterson, J.; Thomson, E.; Network, C. G. A. R.; Sites, T. S.; Ctr, G. S.; Ctr, C. G. C.; Teams, P., Comprehensive genomic characterization defines human glioblastoma genes and core pathways. *Nature* **2008,** *455* (7216), 1061-1068.

29. Wang, J.; Svendsen, A.; Kmiecik, J.; Immervoll, H.; Skaftnesmo, K. O.; Planaguma, J.; Reed, R. K.; Bjerkvig, R.; Miletic, H.; Enger, P. O.; Rygh, C. B.; Chekenya, M., Targeting the NG2/CSPG4 proteoglycan retards tumour growth and angiogenesis in preclinical models of GBM and melanoma. *PLoS One* **2011,** *6* (7), e23062.

30. Svendsen, A.; Verhoeff, J. J.; Immervoll, H.; Brogger, J. C.; Kmiecik, J.; Poli, A.; Netland, I. A.; Prestegarden, L.; Planaguma, J.; Torsvik, A.; Kjersem, A. B.; Sakariassen, P. O.; Heggdal, J. I.; Van Furth, W. R.; Bjerkvig, R.; Lund-Johansen, M.; Enger, P. O.; Felsberg, J.; Brons, N. H.; Tronstad, K. J.; Waha, A.; Chekenya, M., Expression of the progenitor marker NG2/CSPG4 predicts poor survival and resistance to ionising radiation in glioblastoma. *Acta Neuropathol* **2011,** *122* (4), 495-510.

31. Wade, A.; Robinson, A. E.; Engler, J. R.; Petritsch, C.; James, C. D.; Phillips, J. J., Proteoglycans and their roles in brain cancer. *Febs J* **2013,** *280* (10), 2399-2417.

32. Li, C. D.; Wang, K.; Zhou, X. J.; Li, T.; Xu, Y.; Qiang, L.; Peng, M. Z.; Xu, Y. J.; Xie, L.; He, C. L.; Wang, B.; Wang, J. W., Controllable fabrication of hydroxybutyl chitosan/oxidized chondroitin sulfate hydrogels by 3D bioprinting technique for cartilage tissue engineering. *Biomed Mater* **2019,** *14* (2).

33. Abbadessa, A.; Blokzijl, M. M.; Mouser, V. H.; Marica, P.; Malda, J.; Hennink, W. E.; Vermonden, T., A thermo-responsive and photo-polymerizable chondroitin sulfate-based hydrogel for 3D printing applications. *Carbohydr Polym* **2016,** *149*, 163-74.

34. Charles, N.; Ozawa, T.; Squatrito, M.; Bleau, A. M.; Brennan, C. W.; Hambardzumyan, D.; Holland, E. C., Perivascular nitric oxide activates notch signaling and promotes stem-like character in PDGF-induced glioma cells. *Cell Stem Cell* **2010,** *6* (2), 141-52.

35. Calabrese, C.; Poppleton, H.; Kocak, M.; Hogg, T. L.; Fuller, C.; Hamner, B.; Oh, E. Y.; Gaber, M. W.; Finklestein, D.; Allen, M.; Frank, A.; Bayazitov, I. T.; Zakharenko, S. S.; Gajjar, A.; Davidoff, A.; Gilbertson, R. J., A perivascular niche for brain tumor stem cells. *Cancer Cell* **2007,** *11* (1), 69-82.

36. Ricci-Vitiani, L.; Pallini, R.; Biffoni, M.; Todaro, M.; Invernici, G.; Cenci, T.; Maira, G.; Parati, E. A.; Stassi, G.; Larocca, L. M.; De Maria, R., Tumour vascularization via endothelial differentiation of glioblastoma stem-like cells. *Nature* **2010,** *468* (7325), 824-8.

37. Soda, Y.; Marumoto, T.; Friedmann-Morvinski, D.; Soda, M.; Liu, F.; Michiue, H.; Pastorino, S.; Yang, M.; Hoffman, R. M.; Kesari, S.; Verma, I. M., Transdifferentiation of glioblastoma cells into vascular endothelial cells. *P Natl Acad Sci USA* **2011,** *108* (11), 4274-4280.

38. Wang, R.; Chadalavada, K.; Wilshire, J.; Kowalik, U.; Hovinga, K. E.; Geber, A.; Fligelman, B.; Leversha, M.; Brennan, C.; Tabar, V., Glioblastoma stem-like cells give rise to tumour endothelium. *Nature* **2010,** *468* (7325), 829-33.

39. Pietras, A.; Katz, A. M.; Ekstrom, E. J.; Wee, B.; Halliday, J. J.; Pitter, K. L.; Werbeck, J. L.; Amankulor, N. M.; Huse, J. T.; Holland, E. C., Osteopontin-CD44 signaling in

the glioma perivascular niche enhances cancer stem cell phenotypes and promotes aggressive tumor growth. *Cell Stem Cell* **2014,** *14* (3), 357-69.

40. Xie, Y.; Bergstrom, T.; Jiang, Y. W.; Johansson, P.; Marinescu, V. D.; Lindberg, N.; Segerman, A.; Wicher, G.; Niklasson, M.; Baskaran, S.; Sreedharan, S.; Everlien, I.; Kastemar, M.; Hermansson, A.; Elfineh, L.; Libard, S.; Holland, E. C.; Hesselager, G.; Alafuzoff, I.; Westermark, B.; Nelander, S.; Forsberg-Nilsson, K.; Uhrbom, L., The Human Glioblastoma Cell Culture Resource: Validated Cell Models Representing All Molecular Subtypes. *Ebiomedicine* **2015,** *2* (10), 1351-1363.

41. Lakka, S. S.; Gondi, C. S.; Yanamandra, N.; Olivero, W. C.; Dinh, D. H.; Gujrati, M.; Rao, J. S., Inhibition of cathepsin B and MMP-9 gene expression in glioblastoma cell line via RNA interference reduces tumor cell invasion, tumor growth and angiogenesis. *Oncogene* **2004,** *23* (27), 4681-4689.

42. Kenig, S.; Alonso, M. B. D.; Mueller, M. M.; Lah, T. T., Glioblastoma and endothelial cells cross-talk, mediated by SDF-1, enhances tumour invasion and endothelial proliferation by increasing expression of cathepsins B, S, and MMP-9. *Cancer Lett* **2010,** *289* (1), 53-61.

43. Lee, J.; Kotliarova, S.; Kotliarov, Y.; Li, A. G.; Su, Q.; Donin, N. M.; Pastorino, S.; Purow, B. W.; Christopher, N.; Zhang, W.; Park, J. K.; Fine, H. A., Tumor stem cells derived from glioblastomas cultured in bFGF and EGF more closely mirror the phenotype and genotype of primary tumors than do serum-cultured cell lines. *Cancer Cell* **2006,** *9* (5), 391-403.

44. Hidalgo, M.; Amant, F.; Biankin, A. V.; Budinska, E.; Byrne, A. T.; Caldas, C.; Clarke, R. B.; de Jong, S.; Jonkers, J.; Maelandsmo, G. M.; Roman-Roman, S.; Seoane, J.; Trusolino, L.; Villanueva, A., Patient-derived xenograft models: an emerging platform for translational cancer research. *Cancer Discov* **2014,** *4* (9), 998-1013.

45. Wu, M. M.; Swartz, M. A., Modeling Tumor Microenvironments In Vitro. *J Biomech Eng-T Asme* **2014,** *136* (2).

46. Diao, W. W.; Tong, X. Z.; Yang, C.; Zhang, F. R.; Bao, C.; Chen, H.; Liu, L. Y.; Li, M.; Ye, F. F.; Fan, Q. H.; Wang, J. F.; Ou-Yang, Z. C., Behaviors of Glioblastoma Cells in in Vitro Microenvironments. *Sci Rep-Uk* **2019,** *9*.

47. Logun, M. T.; Bisel, N. S.; Tanasse, E. A.; Zhao, W. J.; Gunasekera, B.; Mao, L. D.; Karumbaiah, L., Glioma cell invasion is significantly enhanced in composite hydrogel matrices composed of chondroitin 4-and 4,6-sulfated glycosaminoglycans. *J Mater Chem B* **2016,** *4* (36), 6052-6064.

48. Ananthanarayanan, B.; Kim, Y.; Kumar, S., Elucidating the mechanobiology of malignant brain tumors using a brain matrix-mimetic hyaluronic acid hydrogel platform. *Biomaterials* **2011,** *32* (31), 7913-7923.

49. Grundy, T. J.; De Leon, E.; Griffin, K. R.; Stringer, B. W.; Day, B. W.; Fabry, B.; Cooper-White, J.; O'Neill, G. M., Differential response of patient-derived primary glioblastoma cells to environmental stiffness. *Sci Rep-Uk* **2016,** *6*.

50. Ma, N. K.; Lim, J. K.; Leong, M. F.; Sandanaraj, E.; Ang, B. T.; Tang, C.; Wan, A. C., Collaboration of 3D context and extracellular matrix in the development of glioma stemness in a 3D model. *Biomaterials* **2016,** *78*, 62-73.

51. Martinez-Ramos, C.; Lebourg, M., Three-dimensional constructs using hyaluronan cell carrier as a tool for the study of cancer stem cells. *J Biomed Mater Res B* **2015,** *103* (6), 1249-1257.

52. Heffernan, J. M.; McNamara, J. B.; Borwege, S.; Vernon, B. L.; Sanai, N.; Mehta, S.; Sirianni, R. W., PNIPAAm-co-Jeffamine (R) (PNJ) scaffolds as in vitro models for niche enrichment of glioblastoma stem-like cells. *Biomaterials* **2017,** *143*, 149-158.

53. Wolf, K. J.; Chen, J.; Coombes, J.; Aghi, M. K.; Kumar, S., Dissecting and rebuilding the glioblastoma microenvironment with engineered materials. *Nat Rev Mater* **2019,** *4* (10), 651-668.

54. Ma, J. Y.; Li, N.; Wang, Y. C.; Wang, L.; Wei, W. J.; Shen, L. M.; Sun, Y.; Jiao, Y.; Chen, W. G.; Liu, J., Engineered 3D tumour model for study of glioblastoma aggressiveness and drug evaluation on a detachably assembled microfluidic device. *Biomed Microdevices* **2018,** *20* (3).

55. Wang, C.; Tang, Z.; Zhao, Y.; Yao, R.; Li, L.; Sun, W., Three-dimensional in vitro cancer models: a short review. *Biofabrication* **2014,** *6* (2), 022001.

56. Murphy, S. V.; Atala, A., 3D bioprinting of tissues and organs. *Nat Biotechnol* **2014,** *32* (8), 773-85.

57. Riggs, B. C.; Dias, A. D.; Schiele, N. R.; Cristescu, R.; Huang, Y.; Corr, D. T.; Chrisey, D. B., Matrix-assisted pulsed laser methods for biofabrication. *Mrs Bull* **2011,** *36* (12), 1043-1050.

58. Fernandez-Pradas, J. M.; Florian, C.; Caballero-Lucas, F.; Sopena, P.; Morenza, J. L.; Serra, P., Laser-induced forward transfer: Propelling liquids with light. *Appl Surf Sci* **2017,** *418*, 559-564.

59. Duocastella, M.; Fernandez-Pradas, J. M.; Morenza, J. L.; Serra, P., Time-resolved imaging of the laser forward transfer of liquids. *J Appl Phys* **2009,** *106* (8).

60. Petit, S.; Kerouredan, O.; Devillard, R.; Cormier, E., Femtosecond versus picosecond laser pulses for film-free laser bioprinting. *Appl Opt* **2017,** *56* (31), 8648-8655.

61. Vinson, B. T.; Phamduy, T. B.; Shipman, J.; Riggs, B.; Strong, A. L.; Sklare, S. C.; Murfee, W. L.; Burow, M. E.; Bunnell, B. A.; Huang, Y.; Chrisey, D. B., Laser direct-write based fabrication of a spatially-defined, biomimetic construct as a potential model for breast cancer cell invasion into adipose tissue. *Biofabrication* **2017,** *9* (2).

62. Shah, P. P.; Shah, H. B.; Maniar, K. K.; Özel, T., Extrusion-based 3D bioprinting of alginate-based tissue constructs. *Procedia CIRP* **2020,** *95*, 143-148.

63. Ashammakhi, N.; Ahadian, S.; Xu, C.; Montazerian, H.; Ko, H.; Nasiri, R.; Barros, N.; Khademhosseini, A., Bioinks and bioprinting technologies to make heterogeneous and biomimetic tissue constructs. *Mater Today Bio* **2019,** *1*.

64. Xu, F.; Celli, J.; Rizvi, I.; Moon, S.; Hasan, T.; Demirci, U., A three-dimensional in vitro ovarian cancer coculture model using a high-throughput cell patterning platform. *Biotechnol J* **2011,** *6* (2), 204-212.

65. van Pel, D. M.; Harada, K.; Song, D. D.; Naus, C. C.; Sin, W. C., Modelling glioma invasion using 3D bioprinting and scaffold-free 3D culture. *J Cell Commun Signal* **2018,** *12* (4), 723-730.

66. Wang, X.; Dai, X.; Zhang, X.; Ma, C.; Li, X.; Xu, T.; Lan, Q., 3D bioprinted glioma cell-laden scaffolds enriching glioma stem cells via epithelial-mesenchymal transition. *J Biomed Mater Res A* **2019,** *107* (2), 383-391.

67. Heinrich, M. A.; Bansal, R.; Lammers, T.; Zhang, Y. S.; Michel Schiffelers, R.; Prakash, J., 3D-Bioprinted Mini-Brain: A Glioblastoma Model to Study Cellular Interactions and Therapeutics. *Adv Mater* **2019,** *31* (14), e1806590.

68. Gungor-Ozkerim, P. S.; Inci, I.; Zhang, Y. S.; Khademhosseini, A.; Dokmeci, M. R., Bioinks for 3D bioprinting: an overview. *Biomater Sci-Uk* **2018,** *6* (5), 915-946.

69. Boere, K. W. M.; Blokzijl, M. M.; Visser, J.; Linssen, J. E. A.; Malda, J.; Hennink, W. E.; Vermonden, T., Biofabrication of reinforced 3D-scaffolds using two-component hydrogels. *J Mater Chem B* **2015,** *3* (46), 9067-9078.

70. Hoque, M. E.; San, W. Y.; Wei, F.; Li, S. M.; Huang, M. H.; Vert, M.; Hutmacher, D. W., Processing of Polycaprolactone and Polycaprolactone-Based Copolymers into 3D Scaffolds, and Their Cellular Responses. *Tissue Eng Pt A* **2009,** *15* (10), 3013-3024.

71. Wust, S.; Godla, M. E.; Muller, R.; Hofmann, S., Tunable hydrogel composite with two-step processing in combination with innovative hardware upgrade for cell-based three-dimensional bioprinting. *Acta Biomater* **2014,** *10* (2), 630-40.

72. Souberan, A.; Tchoghandjian, A., Practical Review on Preclinical Human 3D Glioblastoma Models: Advances and Challenges for Clinical Translation. *Cancers (Basel)* **2020,** *12* (9).

73. Chimene, D.; Peak, C. W.; Gentry, J. L.; Carrow, J. K.; Cross, L. M.; Mondragon, E.; Cardoso, G. B.; Kaunas, R.; Gaharwar, A. K., Nanoengineered Ionic-Covalent Entanglement (NICE) Bioinks for 3D Bioprinting. *ACS Appl Mater Interfaces* **2018,** *10* (12), 9957-9968.

74. Peak, C. W.; Stein, J.; Gold, K. A.; Gaharwar, A. K., Nanoengineered Colloidal Inks for 3D Bioprinting. *Langmuir* **2018,** *34* (3), 917-925.

75. Mack, S. C.; Singh, I.; Wang, X.; Hirsch, R.; Wu, Q.; Villagomez, R.; Bernatchez, J. A.; Zhu, Z.; Gimple, R. C.; Kim, L. J. Y.; Morton, A.; Lai, S.; Qiu, Z.; Prager, B. C.; Bertrand, K. C.; Mah, C.; Zhou, W.; Lee, C.; Barnett, G. H.; Vogelbaum, M. A.; Sloan, A. E.; Chavez, L.; Bao, S.; Scacheri, P. C.; Siqueira-Neto, J. L.; Lin, C. Y.; Rich, J. N.,

Chromatin landscapes reveal developmentally encoded transcriptional states that define human glioblastoma. *J Exp Med* **2019,** *216* (5), 1071-1090.

76. Uman, S.; Dhand, A.; Burdick, J. A., Recent advances in shear-thinning and self-healing hydrogels for biomedical applications. *J Appl Polym Sci* **2020,** *137* (25).

77. Klotz, B. J.; Gawlitta, D.; Rosenberg, A. J. W. P.; Malda, J.; Melchels, F. P. W., Gelatin-Methacryloyl Hydrogels: Towards Biofabrication-Based Tissue Repair. *Trends Biotechnol* **2016,** *34* (5), 394-407.

78. Zhou, X.; Zhu, W.; Nowicki, M.; Miao, S.; Cui, H. T.; Holmes, B.; Glazer, R. I.; Zhang, L. G., 3D Bioprinting a Cell-Laden Bone Matrix for Breast Cancer Metastasis Study. *Acs Appl Mater Inter* **2016,** *8* (44), 30017-30026.

79. Liu, W. J.; Zhang, Y. S.; Heinrich, M. A.; De Ferrari, F.; Jang, H. L.; Bakht, S. M.; Alvarez, M. M.; Yang, J. Z.; Li, Y. C.; Trujillo-de Santiago, G.; Miri, A. K.; Zhu, K.; Khoshakhlagh, P.; Prakash, G.; Cheng, H.; Guan, X. F.; Zhong, Z.; Ju, J.; Zhu, G. H.; Jin, X. Y.; Shin, S. R.; Dokmeci, M. R.; Khademhosseini, A., Rapid Continuous Multimaterial Extrusion Bioprinting. *Advanced Materials* **2017,** *29* (3).

80. Liu, W. J.; Zhong, Z.; Hu, N.; Zhou, Y. X.; Maggio, L.; Miri, A. K.; Fragasso, A.; Jin, X. Y.; Khademhosseini, A.; Zhang, Y. S., Coaxial extrusion bioprinting of 3D microfibrous constructs with cell-favorable gelatin methacryloyl microenvironments. *Biofabrication* **2018,** *10* (2).

81. Yin, J.; Yan, M. L.; Wang, Y. C.; Fu, J. Z.; Suo, H. R., 3D Bioprinting of Low-Concentration Cell-Laden Gelatin Methacrylate (GelMA) Bioinks with a Two-Step Cross-linking Strategy. *Acs Appl Mater Inter* **2018,** *10* (8), 6849-6857.

82. Diksin, M.; Smith, S. J.; Rahman, R., The Molecular and Phenotypic Basis of the Glioma Invasive Perivascular Niche. *Int J Mol Sci* **2017,** *18* (11).

83. Hardee, M. E.; Zagzag, D., Mechanisms of Glioma-Associated Neovascularization. *Am J Pathol* **2012,** *181* (4), 1126-1141.

84. Folkins, C.; Shaked, Y.; Man, S.; Tang, T.; Lee, C. R.; Zhu, Z.; Hoffman, R. M.; Kerbel, R. S., Glioma Tumor Stem-Like Cells Promote Tumor Angiogenesis and Vasculogenesis via Vascular Endothelial Growth Factor and Stromal-Derived Factor 1 (vol 69, pg 7243, 2009). *Cancer Research* **2009,** *69* (20), 8216-8216.

85. Montana, V.; Sontheimer, H., Bradykinin Promotes the Chemotactic Invasion of Primary Brain Tumors. *J Neurosci* **2011,** *31* (13), 4858-4867.

86. Trachtenberg, J. E.; Santoro, M.; Williams, C.; Piard, C. M.; Smith, B. T.; Placone, J. K.; Menegaz, B. A.; Molina, E. R.; Lamhamedi-Cherradi, S. E.; Ludwig, J. A.; Sikavitsas, V. I.; Fisher, J. P.; Mikos, A. G., Effects of Shear Stress Gradients on Ewing Sarcoma Cells Using 3D Printed Scaffolds and Flow Perfusion. *Acs Biomater Sci Eng* **2018,** *4* (2), 347-356.

87. Kolesky, D. B.; Homan, K. A.; Skylar-Scott, M. A.; Lewis, J. A., Three-dimensional bioprinting of thick vascularized tissues. *P Natl Acad Sci USA* **2016,** *113* (12), 3179-3184.